The strength of the Earth's magnetic field and the Cretaceous Normal Superchron: New data from Costa Rica

Anita Di Chiara[1], Lisa Tauxe[2], Fabio Florindo[1], Staudigel Hubert[3], Marino Protti[4], Yongjae Yu[5], Jo-Anne Wartho[6], Paul Paul van den Bogaard[6], and Kaj Hoernle[7]

[1]Istituto Nazionale di Geofisica e Vulcanologia
[2]University of California, San Diego
[3]Scripps Institution of Oceanography
[4]Observatorio Vulcanológico y Sismológico de Costa Rica
[5]Chungnam National University
[6]GEOMAR Helmholtz Centre for Ocean Research Kiel
[7]GEOMAR Helmholtz Center for Ocean Research Kiel

November 24, 2022

Abstract

Constraining the long-term variability and average of the Earth's magnetic field strength is fundamental to understanding the characteristics and behavior of the geomagnetic field. Questions remain about the strength of the average field, and the rela-tionship between strength and reversal frequency. The dispersion of data from key timeintervals reflects the complexity in obtaining absolute paleointensity values. Here, we focus on the Cretaceous Normal Superchron (CNS; 121-84 Ma), during which there were no reversals. We present new results from 42 submarine basaltic glass (SBG) sites collected on the Nicoya Peninsula and Murcielago Islands, Costa Rica and new and revised 40Ar/39Ar ages along with biostratigraphic age constraints from previous studies that indicate ages from 141 to 112 Ma. One site with a 40Ar/39Ar age of 135+\-1.5Ma (2σ) gave a reliable intensity result of 34+\-µT (equivalent to a paleomagnetic dipole moment, PDM, value of 88+\-20 ZAm2), while three sites between 121 and 112 vary from 21+\- to 34+\-4 µT (53+\-3 to 87+\-10 ZAm2) spanning the onset of the CNS. These results from the CNS are all higher than the long-term average of ˜42 ZAm2 and similar to data from Suhongtu (46-53 ZAm2) and the Troodos Ophiolite (81 ZAm2, reinterpreted, using the same criteria of this study). Together with the reinterpreted data, the new Costa Rica results suggest thatthe strength of the geomagnetic field was about the same before and after the onset ofthe CNS. Therefore, the data do not support a strict correlation between polarity interval length and the strength of the magnetic field.

Table DR1 - Summary table of $^{40}Ar/^{39}Ar$ analyses from Costa Rica

Sample #	Material	Laboratory ID #	Plateau age ± 2σ (Ma)[a]	MSWD	P %	% ^{39}Ar	Steps	Inverse isochronage ± 95% conf. (Ma)[a]	Initial $^{40}Ar/^{36}Ar$	MSWD	P %	SF %	Steps	% $^{40}Ar_{atm}$ range	Comments
CR01	Basaltic glass	CR1gls	**131.0 ± 3.2**	0.41	93	61.0	6-15	130 ± 11	297 ± 12	0.48	87	*25.1*	6-15	26-99	Disturbed age spectrum, high Cl in steps 1-,4-20, steps 2-3 have >10 V ^{40}Ar.
CR03	Basaltic glass	CR3gls	**130.0 ± 4.5**	0.41	96	67.8	6-18	136 ± 11	288 ± 13	0.33	98	41.0	6-18	35-99	Slightly disturbed age spectrum, high Cl in steps 4-18, steps 1-3 have >10 V ^{40}Ar.

The bold values indicate the preferred ages, and italics indicate statistically invalid values (i.e., MSWD < 0.30, P < 5 %, or SF = < 40%).

[a]The plateau ages are quoted with 2σ internal errors, and the inverse isochron ages of the plateau steaps are quoted with 95% confidence errors (i.e., internal errors multipled by √MSWD and t Student's test with n-1 degrees of freedom).

Abbreviations: MSWD = Mean Square Weighted Deviation, P = probability, SF = spreading factor, plateau age = > 50% total ^{39}Ar, and $^{40}Ar^{atm}$ = atmospheric ^{40}Ar.

The strength of the Earth's magnetic field and the Cretaceous Normal Superchron: New data from Costa Rica

A. Di Chiara[1,2], L. Tauxe[2], H. Staudigel[2], F. Florindo [1], M. Protti[3], Y. Yu[4], J-A. Wartho [5], Paul van den Bogaard [5], K. Hoernle[5,6]

[1]Istituto Nazionale di Geofisica e Vulcanologia, Rome, Italy
[2]Scripps Institution of Oceanography, La Jolla, CA
[3]Observatorio Vulcanológico y Sismológico de Universidad Nacional de Costa Rica, Costa Rica
[4]Department of Geological Sciences, Chungnam National University, Daejeon, 34134, Korea
[5]GEOMAR Helmholtz Centre for Ocean Research Kiel, 24148 Germany
[6]Kiel University, 24118 Germany

Key Points:

- The Cretaceous Normal Superchron (CNS) is key to understanding geomagnetic field behavior
- We present new paleointensity data from Costa Rica from 135 to 112 Ma, spanning the onset of the CNS
- We find that field strength was high both prior and during the early CNS, thus negating a correlation between field strength and stability

Corresponding author: Anita Di Chiara, `dichiaraanita@gmail.com`

Abstract

Constraining the long-term variability and average of the Earth's magnetic field strength is fundamental to understanding the characteristics and behavior of the geomagnetic field. Questions remain about the strength of the average field, and the relationship between strength and reversal frequency. The dispersion of data from key time intervals reflects the complexity in obtaining absolute paleointensity values. Here, we focus on the Cretaceous Normal Superchron (CNS; 121-84 Ma), during which there were no reversals. We present new results from 42 submarine basaltic glass (SBG) sites collected on the Nicoya Peninsula and Murciélago Islands, Costa Rica and new and revised ^{40}Ar/^{39}Ar ages along with biostratigraphic age constraints from previous studies that indicate ages ranging from 141 to 112 Ma. One site with a ^{40}Ar/^{39}Ar age of 135 ± 1.5 Ma (2σ) gave a reliable intensity result of 34 ± 8 μT (equivalent to a paleomagnetic dipole moment, PDM, value of 88 ± 20 ZAm^2), while three sites between 121 and 112 vary from 21 ± 1 to 34 ± 4 μT (53 ± 3 to 87 ± 10 ZAm^2) spanning the onset of the CNS. These results from the CNS are all higher than the long-term average of ∼42 ZAm^2 and similar to data from Suhongtu (46-53 ZAm^2) and the Troodos Ophiolite (81 ZAm^2, reinterpreted using the same criteria of this study). Together with the reinterpreted data, the new Costa Rica results suggest that the strength of the geomagnetic field was about the same before and after the onset of the CNS. Therefore, the data do not support a strict correlation between polarity interval length and the strength of the magnetic field.

Plain language summary

Understanding the Earth's magnetic field behavior in the past is important for geodynamo simulations. However, because of the paucity of available data, it is poorly understood. In particular, it has been argued that the strength of the Earth's magnetic field, or paleointensity, seems correlated with the stability of the field, where a strong field may be less prone to magnetic reversals than a weak field. Hence, we have investigated the anomalously long period of stability, the Cretaceous Normal Superchron (CNS) during which no magnetic reversals occurred. Our new data from Costa Rica basaltic glasses, together with reinterpreted data from the Suhongtu lavas in Mongolia, Troodos ophiolite in Cyprus suggest that the magnetic field during the CNS was similar to the present day field and these high values are nearly twice the long-term average value. However, high field values were also detected in the period prior to the onset of the CNS as well, hence our data do not support a strict correlation between strength and stability of the Earth's magnetic field.

1 Introduction

From the analysis of satellite data, we observe a rapid decrease of the present-day Earth's magnetic (geomagnetic) field strength (intensity), thus raising the question of whether we are approaching a polarity reversal (e.g. Hulot et al., 2002; Pavón-Carrasco & De Santis, 2016) or not (Brown et al., 2018). Constraining the past evolution of intensity (paleointensity) can provide context for this scenario, and help us to understand fundamental properties of the geomagnetic field, such as the long-term average dipole moment and how the field's strength is related to reversals, reversal frequency and secular variation (e.g. Cox, 1968).

Generally, paleointensity minima are associated with magnetic excursions and reversals but they are not always associated with these events (Channell et al., 2020). Identifying a relationship between dipole strength and magnetic reversals (Biggin & Thomas, 2003; Biggin et al., 2012; Constable et al., 1998; Cox, 1968; Ingham et al., 2014; Kulakov et al., 2019; Larson & Olson, 1991; Loper & McCartney, 1986; McElhinny & Larson, 2003; Prévot et al., 1990; Selkin & Tauxe, 2000; Tarduno et al., 2001; Tarduno & Cottrell, 2005;

Tauxe, 2006; Tauxe et al., 2013; Tauxe & Yamazaki, 2015; Thomas et al., 1998, 2000) would provide important constraints on the heat flux across the Earth's core-mantle boundary and the energy states of the geodynamo. These in turn would have significant implications for the geodynamo and mantle modeling (Biggin et al., 2012). Moreover, understanding the long-term variations of the geomagnetic field strength (McFadden & McElhinny, 1982; Juarez et al., 1998; Wang et al., 2015; Tauxe et al., 2013; Kulakov et al., 2019; Ingham et al., 2014) over thousands to millions of years is not only fundamental for modelling the geodynamo origin and behavior (e.g. Biggin et al., 2012) but also for other applications, such as estimating the solar standoff distance (Tarduno et al., 2014) or geodynamic plate reconstructions (e.g. Olierook et al., 2020). However, there is no consensus yet as to the average strength of the geomagnetic field, with estimates ranging from 80 $\pm$ 7 ZAm^2 (where ZAm^2 =10^{21} Am^2) for the last 5 Ma (McFadden & McElhinny, 1982), to 42 $\pm$ 23 ZAm^2 for the last 160 Ma (all intensity values errors are 1σ; Juarez et al., 1998).

Despite the many compilations associated with the strength of the geomagnetic field over time (e.g. Biggin & McCormack, 2010; Perrin & Schnepp, 2004; Perrin & Shcherbakov, 1997; Tanaka et al., 1995; Tauxe & Yamazaki, 2015, and earthref.org/MagIC), the data distribution is uneven both geographically and temporally. Overall, $\sim$95% of the data in the MagIC database (combining both volcanic and archeomagnetic records) comes from northern hemisphere locations, whereas only $\sim$5% comes from southern latitudes. Moreover, most of the data comes from the last 20,000 years. This significant bias in geographic and temporal span is due to: i) the limited availability of suitable materials for paleomagnetic analyses, as older rocks with ideal characteristics are much less common than younger rocks, and ii) the high-failure rate and time-consuming nature of the paleointensity experiments. The scatter in the database may be also increased by low resolution of geochronological dating methods (the uncertainties can range from hundreds to millions of years).

A way to advance our understating of geomagnetic field activity and mantle dynamics is to investigate the superchrons, intervals of tens of millions of years that lack reversals. Gubbins (1999) proposed that excursions and reversals nucleate in the fluid outer core and if the reverse outer core field is maintained for longer than about 3 ka (the magnetic diffusion time of the inner core) then the field is able to diffuse into the inner core, allowing the dipole field to reverse. This hypothesis may explain the existence and relatively short duration of the magnetic excursions, which are thousands of years long. In contrast, superchrons may be related to the relationship between the Earth's dynamo and the lower mantle (Glazmaier et al., 1999; Larson & Olson, 1991; Olson et al., 2012) or they can be triggered by crustal/upper mantle events, such as an impingement of a subducted slab with the core–mantle boundary (Courtillot et al., 2007; Larson & Olson, 1991).

If the long-term thermal effect of mantle convection on the core during the Cretaceous led to a gradual decrease of the reversal rate before the onset of the superchron, then its existence could be predicted (McFadden & McElhinny, 1984; McFadden & Merrill, 2000). Alternatively, if the reversal rate was stationary before the superchron (Gallet & Hulot, 1997; Hulot & Gallet, 2003), then it could represent a sudden non-linear transition between a reversing and a non-reversing state of the geodynamo and the CNS could not be predicted (de-coupling between core-mantle processes and geomagnetic field long term changes, Prévot et al., 1990). Furthermore, numerical simulations by Olson and Hagay (2015) suggested that superchrons are induced by mantle 'superplume' activity. These are manifested by major Large Igneous Provinces (LIPs), the age of which post-date transitions from hyper-reversing (i.e. the Jurassic Hyperactivity Period, JHP, Kulakov et al., 2019) to superchron geodynamo states (i.e., the CNS). Therefore, improving our knowledge of the timing and extent of LIPs could help constraining the geomagnetic field behavior. Finding a precursor event to a superchron would support one of the competing hypotheses over the others (Gallet & Hulot, 1997; Hulot & Gallet, 2003; Zhu, Hoffman, et al., 2004). The key to this is to expand the existing sparse database spanning the onset of a superchron (here the CNS). In this study, we focus on obtaining new and robust data from before and after the onset of the CNS, from the study of part of the Caribbean Large Igneous Province (CLIP: e.g., Boshman et al., 2019) in Costa Rica.

2 The Cretaceous Normal Superchron (CNS)

The Cretaceous Normal Superchron (C34n; informally called 'the Cretaceous quiet zone', e.g., Gee & Kent, 2007) is a long period of nearly uniform normal polarity, first observed by Helsley and Steiner (1968) in ocean-floor magnetic anomaly profiles. The CNS began between 123.0 and 121.2 Ma, with a duration of 38.0 to 40.5 Ma (see review by Olierook et al., 2020), and it provides a unique opportunity to investigate the geomagnetic field behavior before, during, and after a superchron. Indeed, the CNS is preceded by the so-called 'Mesozoic dipole low' (Prévot et al., 1990) with an average intensity value of ∼32 ZAm^2 (e.g. Tauxe et al., 2013), possibly linked to a change of state of the geomagnetic field from a state of relatively rapid reversals, to a period of stability during the CNS. Cox (1968) suggested that when the field is stronger, it is also more stable and therefore the frequency of reversals should be lower. Many subsequent studies have supported the inverse correlation between field strength and reversal frequency (e.g. Constable et al., 1998; Tauxe & Hartl, 1997; Tauxe & Staudigel, 2004; Tauxe, 2006; Tauxe & Yamazaki, 2015; Kulakov et al., 2019), whereas others (e.g. Selkin & Tauxe, 2000) suggested that the distribution of paleointensities does not change substantially between a low reversal-rate period (e.g., between 124 and 30 Ma) and a high reversal-rate period (e.g., between 30 and 0.3 Ma).

At present, too few data are available to rule out either of these hypotheses, as suggested by Ingham et al. (2014). The investigation of SBG samples from the Troodos ophiolite in Cyprus (92 Ma, Tauxe & Staudigel, 2004) suggest that a strong and stable field was present during the CNS, with a mean dipole moment of 81 ± 43 ZAm^2. An even higher dipole moment values of 125 ± 14 ZAm^2 was recovered from single plagioclase crystals extracted from the Rajmahal Traps of India (113 to 116 Ma; Cottrell & Tarduno, 2000; Tarduno et al., 2001) and 127 ± 7 ZAm^2 from the Canadian Arctic Ellesmere Island 95 Ma lavas (Tarduno et al., 2002). High values were later supported by the review of paleointensity data from all SBG samples (up to 2006) from Deep Sea Drilling Project and Ocean Drilling Program (DSDP/ODP) core samples (Tauxe, 2006).

Alternatively, there are many studies that suggest relatively low field values during the whole period of the CNS. Data from the lower crust (gabbros) of the Troodos ophiolite by Granot et al. (2007) pointed to fluctuations of the intensities around a mean of 54 ± 20 ZAm^2, which are weaker and more variable than predicted by geodynamo simulations. Low intensity values were also observed from the 114-110 Ma Suhongtu lava section (Inner Mongolia) by Zhu et al. (2008) who found a field that fluctuated from 53 ± 20 ZAm^2 to 46 ± 27 ZAm^2. Similar low intensity values were also found by Pick and Tauxe (1993a) after analyzing SBG samples from the East Pacific Rise DSDP/ODP sites spanning the onset of the CNS (Holes 417D, 418A, 807C), and near the CNS termination (Hole 543A). A precursor event to the CNS has been proposed by Gallet and Hulot (1997) and Hulot and Gallet (2003), and supported by values of 64 ± 23 ZAm^2 at 134 Ma from Uruguay (e.g. Goguitchaichvili et al., 2008). Moreover, data from the Zhuanchengzi in Liaoning Province, K-Ar dated at 120.93 ± 0.88 Ma (all age uncertainties are 2σ unless otherwise stated) closely following the onset of the CNS, reveal a low average intensity of 39.6 ± 0.8 ZAm^2 (Zhu et al., 2001). An even weaker field was reported from the southern hemisphere, with data from 135 Ma old lava flows from the Etendeka-Paraná Province (Dodd et al., 2015), with an average of 25 ± 10 ZAm^2. Similar low values of 41 ± 16 ZAm^2 (and high variability) were found on the South American part of the same province, in the 130 Ma Ponta Grossa tholeiitic dykes (Cejudo Ruiz et al., 2009), from a sequence of 124-133 Ma lava flows at Sihetun (Zhu et al., 2004a) and 122 Ma andesitic basalt lava flows from Hulahada, northeastern China (Zhu et al., 2004b). Thus, these data (Zhu et al., 2001, 2003; Zhu, Lo, et al., 2004; Cejudo Ruiz et al., 2009; Dodd et al., 2015) suggest that no precursor to the CNS was recorded and the field was weak both prior to (35.3 $\pm$ 0.2 ZAm^2) and after (48 $\pm$ 0.2 ZAm^2) the CNS. These low intensities would support a decoupling of the processes controlling reversal frequency and paleointensity.

There is also a discrepancy between magnetic anomalies, volcanic and sedimentary data (Tarduno, 1990; Cronin et al., 2001; Granot et al., 2012) during the CNS. For example, Granot et al. (2012) discovered two magnetic anomalies within the CNS (with higher intensity values at $\sim$108 Ma, and lower at $\sim$92 Ma) from deep-tow magnetic profiles from the Central Atlantic Ocean, which are not observed in the volcanic or sedimentary data.

Kulakov et al. (2019) analyzed data from the PINT (Paleo-INTensity) dataset (Biggin & McCormack, 2010), to investigate the variability of the geomagnetic field and reversal frequency between the CNS and the JHP; they found a weak inverse correlation using the entire dataset, which is in agreement with Channell et al. (1982) and Tarduno and Cotrell (2005). However, when using a stricter selection criteria, no correlation was found. Overall, Kulakov et al. (2019) found an increase of field strength at $\sim$133 Ma, before the onset of the CNS, which lasted up to 15 Ma after the end of the CNS, and two peaks at $\sim$117 and $\sim$95 Ma, reminiscent of the findings of Granot et al. (2012). Kulakov et al. (2019) also pointed out that material from which the paleointensity data were recovered may also bias the results as data from single zircons are systematically higher with less variability compared to data from SBG and whole rock samples, while SBG give more dispersed values with lower median values. However, we note that overall there are very few single crystal results and the results have never been verified by measuring samples cooled in known fields, whereas SBG has been verified multiple times.

SBG is rapidly cooled, is likely to have single domain magnetic particles (Pick & Tauxe, 1993a, 1993b; Bowles et al., 2005), and may yield results that meet stricter criteria than in other materials. SBG has been the subject of many paleointensity studies (e.g. Bowles et al., 2005; Juarez et al., 1998; Juarez & Tauxe, 2000; Pick & Tauxe, 1993a; Riisager et al., 2003; Selkin & Tauxe, 2000; Smirnov & Tarduno, 2003; Tauxe & Staudigel, 2004; Tauxe et al., 2013) and their reliability has been thoroughly discussed. For instance, Smirnov and Tarduno (2003) compared the rock magnetic properties and behavior of a few specimens during heating (as required for running Thellier experiments) on Holocene and Cretaceous SBG and concluded that the magnetic behavior of their specimens was not comparable, pointing out that partial melting and neo-crystallization of magnetic grains would bias the results toward lower values. On the other hand, Tauxe and Staudigel (2004) argued that SBG are resistant under some conditions; indeed, the susceptibility of volcanic glasses to weathering may cause the alteration of the glass into hydrous phases that would in turn rapidly disappear from the geological record. Nonetheless, fresh-looking samples are still found in abundance in outcrops (e.g. Tauxe & Staudigel, 2004) and drill cores (e.g. Selkin & Tauxe, 2000; Tauxe, 2006). These glasses also give paleointensity results that meet strict criteria, thus suggesting magnetic stability over millions of years. In contrast, Heller et al. (2002) argued for a low temperature origin of low-Ti titanomagnetite, because it cannot be found as equilibrium phase in Mid Oceanic Ridge basalts. However, three important pieces of evidence argue otherwise: 1) low-Ti titanomagnetite is found in freshly erupted material, 2) several successful paleointensity experiments from historical flows clearly show blocking temperatures from 430 to 575°C (Bowles et al., 2011; Carlut & Kent, 2000; Juarez et al., 1998; Kent & Gee, 1996; Pick & Tauxe, 1993a; Tauxe et al., 2013), which yielded values in good agreement with the known field from the eruptions, and 3) glass is by definition not an equilibrium material, so the argument of Heller et al. (2002) is irrelevant. Finally, as volcanic glasses cool rapidly (are quenched) below the Curie temperatures (Bowles et al., 2005), little or no cooling rate correction needs to be applied to the final data when acquired by rapid cooling (as observed in the Scripps Paleomagnetic Laboratory).

Here, we present new and robust results obtained from SBG samples from Costa Rica (the Nicoya Peninsula and Murciélago Islands). These new data, combined with previous studies that provided geochronological and biostratigraphic ages between 141 and 94 Ma, give us the opportunity to investigate the geomagnetic field field strength before and during the CNS.

3 Geological setting and sampling

Costa Rica is located near the triple junction of the Cocos, Caribbean and Nazca plates (DeMets, 2001), where the Cocos Plate subducts beneath the Caribbean Plate at a rate of ∼8.5 cm yr^{-1}. For this study, we focus on the Nicoya Peninsula and Murciélago islands in the north west (10° N; 85° W, Figure 1), where an important ophiolitic complex exposes upper crust sequences and overlying sediments. The Nicoya Peninsula comprises Cretaceous aphyric pillow lavas and lava flows (dated by $^{40}Ar/^{39}Ar$), which are associated with the formation of the Jurassic-Cretaceous CLIP (Sinton et al., 1997; Hauff et al., 2000; Hoernle et al., 2004; Madrigal et al., 2016). The crustal basaltic sequence is locally intruded by late Cretaceous diabases, gabbros and plagiogranites dated by $^{40}Ar/^{39}Ar$ and U-Pb methods (Hauff et al., 2000; Madrigal et al., 2016; Sinton et al., 1997; Whattam & Stern, 2016) and by analyses of dismembered radiolaritic chert sequences from the Middle Jurassic to Late Cretaceous (Baumgartner, 1984; Schmidt-Effing, 1975, 1979; Bandini et al., 2008; Baumgartner et al., 1995). There are rare occurrences of fossil-bearing intra-pillow sediments indicating an age of ∼94 Ma (Azema et al., n.d.; Tournon & Alvarado, 1997).

Three extrusive lava sequences are recognised, which are chronologically divided into three main events: Nicoya I (∼140 Ma), Nicoya II (∼120 Ma) and Nicoya III (∼90 Ma; Hoernle et al., 2004; Madrigal et al., 2016). These are considered to be part of the CLIP and a remnant of the Panthalassa Ocean. The lava sequences preserve fresh pillow-rim glasses (Figures 1 and 2). The lack of vescicularity in the lava flows and the high sulfur concentrations (1000—2000 ppm S; Hauff et al., 1997) in these fresh glasses from pillow rims indicate low degrees of degassing. Therefore, they likely erupted in moderate to deep water depths (Moore & Schilling, 1973). In most of the sites, the thickness of the cooling units (up to 50 m) and the paucity or lack of primary sediment intercalations suggests high eruption rates over relatively short time intervals, thus ensuring good preservation and little to no post-eruptive alteration of the volcanic deposits.

The ophiolitic complex is overlain in the north by Middle Campanian-Maastrichtian shallow-water carbonate deposits (e.g. Baumgartner-Mora & Denyer, 2002), and in the center by Albian black shales and Coniacian-Campanian pelagic to turbiditic sequences. The Murciélago Islands, north of the Nicoya Peninsula, are not considered part of the Santa Helena ophiolite located to the east, because the basalts are geochemically almost identical to the CLIP and the older basaltic suites of the Nicoya Peninsula (Escuder-Viruete et al., 2015; Madrigal et al., 2015).

Two sample collections were available for this study: the CR and NC collections (Table 1 and Figure 1). The CR collection consists of 10 sites of pillow rinds and hyaloclastites. Sites CR01-04 were collected from outcrops along the beach east of Playa del Coco and from the same tectonic block. In this study, we present new $^{40}Ar/^{39}Ar$ dates from sites CR01 (131.0 ± 3.2 Ma) and CR03 (130.0 ± 4.5 Ma). Additional $^{40}Ar/^{39}Ar$ ages are available from this area. We have recalculated them using consistent age standards and K decay constants (Fleck et al., 2019). These recalculated published ages include 141.4 ± 1.1 Ma (originally 139.1 ± 1.1 Ma; sample AN8 by Hoernle et al., 2004), 139.9 ± 1.8 Ma (originally 137.6 ± 1.8 Ma; sample AN10 by Hoernle et al., 2004) and 136.5 ± 2.5 Ma (originally 137.1 ± 2.5 Ma; sample NI7 by Madrigal et al., 2016). Thus, we use a weighted mean age of 140.99 ± 0.94 Ma (Mean Squares Weighted Deviation (MSWD) =2.0, Probability (P)=15%, from close-proximity samples AN8 and AN10; Hoernle et al., 2004) for the CR02 and CR04 sites. Sites CR05 and CR06 are from northeast of Playa Hermosa, in the same location as the BN22 site dated at 112.4 ± 0.9 Ma (originally 110.6 ± 0.9 Ma; Hoernle et al., 2004). Samples CR13 and CR14 are from western Playa del Coco, both from the same pillow lava sequence dated at 135.1 ± 1.5 Ma (originally 132.9 ± 1.5 Ma; sample AN3 by Hoernle et al., 2004). In the central-western coast, site CR18 is dated at 121.4 ± 1.1 Ma (originally 119.4 ± 1.1 Ma; sample AN34 from Hoernle et al., 2004). Further south, site CR20 has a slightly younger age of 120.2 ± 1.8 Ma (originally 118.2 ± 1.8 Ma; sample AN40 from Hoernle et al., 2004). Sites NC17-18 and NC19-28 from this study were collected at the same locations as CR18 and CR19-CR20, respectively. The NC sample set (Figures 1 and 2) consists of 38 single pillow basalts, where each pillow represents a sampling site. Fragments of fresh basaltic glass were collected from pillow rinds (Table 1, Figures 1 and 2). The ages of the NC collection were assigned using their close-proximity to dated sites from previous studies (Table 1, Figure 1). From the north of the Nicoya Peninsula, in the Murciélago Islands, we collected samples from five sites, NC01-05; NC01 and NC03-05 with a close-proximity $^{40}Ar/^{39}Ar$ age of 110.6 ± 2.0 Ma (originally 109.0 ± 2.0 Ma; sample SE6 from Hauff et al., 2000) and site NC02 with an age of 113.0 ± 3.5 Ma (originally 113.4 ± 3.5 Ma; sample SE-050611-11 from Madrigal et al., 2016). From north to south on the Nicoya Peninsula, 29 sites (NC06-34) were collected. Sites NC31-32 were dated at 94 Ma (based on close-proximity to a radiolaria biostratigraphic age from site NB03; Tournon & Alvarado, 1997). Site NC33 was dated at 96.1 ± 0.9 Ma (originally 94.7 ± 0.9 Ma, based on nearby site AN86 of Hauff et al., 2000) and finally from the south, at Quepos, sites NC36-38 were dated at 64.7 ± 0.5 Ma (originally 63.9 ± 0.5 Ma, based on the close-proximity to sample S-QP93-1; Sinton et al., 1997).

4 Methods and results

In this study, we analysed a total of 360 specimens from 42 sites using the IZZI method of Yu et al. (2004). Tauxe and Staudigel (2004) used this method to study SBG samples from the Troodos Ophiolite in Cyprus. The IZZI protocol embeds two variations of the Thellier-Thellier method: the in-field, zero-field (IZ) method of Aitken et al. (1988) and the zero-field, in-field (ZI) method of Coe (1967) with the addition of the so-called partial Thermal Remanent Magnetization (pTRM) checks of Coe et al. (1978). This approach ensures a built-in check for alteration during the experiments and a test of the so-called 'Reciprocity Law' of Thellier and Thellier (1959).

Between 8 to 20 SBG specimens were analysed per site, following the suggestion of Santos and Tauxe (2019) that if an experiment contains a sufficient number of specimens, the field estimate is affected by a large bias. In this study, we performed 20 to 48 heating steps per experiment in four experiments with three different laboratory fields (15, 25 and 45 μT).

Data were analysed using the PmagPy software package (Tauxe et al., 2016). The Natural Remanent Magnetization (NRM) values remaining after each heating step were plotted against the pTRM gained in Arai plots (Nagata et al., 1963) along with corresponding Zijderveld (Zijderveld, 1967), equal area, magnetization versus temperature (M/T) and site level plots (Figure 3). The criteria used in this study were used as threshold values to select the most reliable and straight Arai plots and were similar to the strict CCRIT set of Cromwell et al. (2015) and Tauxe et al. (2016). Acceptable (successful) specimens were characterized by three or more pTRM checks (N_{pTRM}); a Fraction of Remanence (FRAC) value used in the slope calculation (defined by Paterson et al. (2014)) of greater than or equal to 0.78, SCAT (=True), *b_beta* value greater than 0.1, MAD and DANG

Site	Location	Type	Lat (°N)	Long (°W)	Age (Ma)	2σ	Ref.
NC01	N of Isla San Pedrito	glassy pm	10.856	85.952	113.0	3.5	3
NC02	Golondrina Island	pm	10.856	85.944	113.0	3.5	3
NC03	San Jose Island	pm	10.854	85.926	113.0	3.5	3
NC04	Cocinera Island	SBG	10.857	85.907	110.6	2.0	2
NC05	San Jose Island	SBG	10.851	85.912	113.0	3.5	3
NC06	N of P. Guacamaya	SBG	10.533	85.781	[-]	[-]	[-]
NC07	P. Junquillal/ Hermosa	fine pm	10.154	85.808	[-]	[-]	[-]
NC08	P. Blanca	SBG	10.181	85.821	[-]	[-]	[-]
NC09A	Venado	SBG	10.128	85.798	[-]	[-]	[-]
NC09B	Venado	SBG	10.127	85.797	[-]	[-]	[-]
NC10A	La Joya del Lagarto	SBG	10.112	85.794	[-]	[-]	[-]
NC10B	La Joya del Lagarto	fine pm	10.112	85.795	[-]	[-]	[-]
NC11	Near NC10	SBG	10.108	85.794	[-]	[-]	[-]
NC12A	P. Nilo	pm	10.105	85.791	[-]	[-]	[-]
NC12B	P. Nilo	hyalo.	10.105	85.791	[-]	[-]	[-]
NC13	N of P. Pitahaya	SBG	10.067	85.77	[-]	[-]	[-]
NC14	between P. Nilo & P. Frijolar	hyalo.	10.095	85.789	[-]	[-]	[-]
NC15	near NC14	SBG	10.095	85.789	[-]	[-]	[-]
NC16	near NC15	SBG	10.093	85.787	[-]	[-]	[-]
NC17	San Juanillo	SBG	10.034	85.739	121.4	1.1	1
NC18	Punta Islita	SBG	9.85	85.404	121.4	1.1	1
NC19	Punta Islita	SBG	9.848	85.402	120.2	1.8	1
NC20	Punta Islita	SBG	9.848	85.403	[-]	[-]	[-]
NC21	Punta Islita	SBG	9.848	85.403	[-]	[-]	[-]
NC22	P. Corozalito	SBG	9.846	85.383	120.2	1.8	1
NC23	P. Corozalito	glassy pm	9.848	85.383	120.2	1.8	1
NC24	P. Corozalito	glassy pm	9.849	85.382	120.2	1.8	1
NC25	P. Corozalito	glassy pm	9.844	85.374	120.2	1.8	1
NC26	camping Corozalito	glassy pm	9.845	85.374	120.2	1.8	1
NC27	camping Corozalito	glassy pm	9.845	85.373	120.2	1.8	1
NC28	camping Corozalito	glassy pm	9.845	85.374	120.2	1.8	1
NC29	P. Bejuco		9.823	85.331	120.2	1.8	1
NC30	Punta coyote		9.76	85.275	[-]	[-]	[-]
NC31	P. Las Manchas	pm	9.644	85.073	94	[-]	5
NC32	P. Las Manchas		9.646	85.072	94	[-]	5
NC33	Ballena Bay		9.737	84.977	96.1	0.9	2
NC34	P. Posa Colorada	glassy pm	9.788	84.922	[-]	[-]	[-]
NC35	P. Los Muertos	glassy pm	9.76	84.893	[-]	[-]	[-]
NC36	P. Espadilla	weathered p.	9.389	84.148	64.7	0.5	4
NC37	P. Espadilla	p. breccia	9.388	84.147	64.7	0.5	4
NC38	P. Las Gemelas	fine grained	9.38	84.14	64.7	0.5	4
CR01	Punta Cacique	hyalo.	10.566	85.693	131.0	1.6	TS
CR02	Punta Cacique	glassy pm	10.569	85.7	141.0	0.9	1/TS
CR03	Punta Cacique	hyalo.	10.571	85.687	130.0	4.5	TS
CR04	Punta Cacique	hyalo.	10.569	85.685	141.0	0.9	1/TS
CR05	NE of P. Hermosa	glassy pm	10.589	85.68	112.4	0.9	1
CR06	near CR5	glass pm	10.588	85.679	112.4	0.9	1
CR13	Punta Miga	hyalo.	10.555	85.709	135.1	1.5	1
CR14	Punta Miga	glassy pm	10.55	85.707	135.1	1.5	1
CR18B	P. San Juanillo	glassy pm	10.029	85.739	121.4	1.1	1
CR20B	P. Corozalito	hyalo.	9.848	85.383	120.2	1.8	1

Table 1. Site, location name and coordinates. Abbreviations: pm=pillow margin; SBG= submarine basaltic glass; hyalo.= hyaloclastite; P= playa; Lat.= Latitude; Lon= Longitude; Ref.= Reference.The literature $^{40}Ar/^{39}Ar$ ages were recalculated using the standard ages and K decay of Fleck et al. (2019). Reference 1= Hoernle et al., 2004; 2= Hauff et al., 2000; 3= Madrigal et al., 2016; 4= Sinton et al., 1997; 5= Tournon & Alvarado, 1997 (radiolaria biostratigraphic age); and TS= this study.

values of lower than or equal to 10, and a $|\vec{k'}|$ (the curvature value of Paterson, 2011, evaluated over the selected interval) of less than or equal to 0.164. For a few specimens with clear two component behavior in the directions, we allowed the FRAC value to be as low as 0.3 (CCRIT-relaxed), and used the slope of the line associated with the characteristic component. For a complete definition of the selection criteria we refer to the paper of Paterson et al. (2014). The selection criteria at site level required that the number of successful specimens per site ($N_{spec.}$) was greater than 3 and the standard deviation was lower than 10 μT.

4.1 ^{40}Ar/^{39}Ar methods and results

^{40}Ar/^{39}Ar dating was undertaken on two basaltic glass samples (CR01 and CR03) at the Argon Geochronology in Oceanography (ArGO) Laboratory at GEOMAR Helmholtz Centre of Ocean Research Kiel. A detailed description of the methods and equipment used can be found in Homrighausen et al. (2019) and the full data is presented in Tables DR1 and DR2 (Supplementary material). The samples were irradiated for 168 hours at 5 MW, in the C6 position of the GKSS nuclear reactor, Germany. Aliquots of the Taylor Creek sanidine age standard (TCs; 28.344 ± 0.011 Ma (1σ; Fleck et al., 2019) were co-irradiated with the unknown samples, and the K(total) decay constant of Steiger and Jäger (1977) was used. In order to robustly compare our new data with the literature's ^{40}Ar/^{39}Ar ages, the ages of Sinton et al. (1997), Hauff et al. (2000), Hoernle et al. (2004), and Madrigal et al. (2016) were recalculated utilizing the ArAR calculator of Mercer and Hodges (2016), using the total ^{40}K(total) decay constant of Steiger and Jäger (1977), as per the recommendation of Fleck et al. (2019). The following standard ages were also applied to the previously published ^{40}Ar/^{39}Ar data: a TCs age of 28.344 ± 0.011 Ma (1σ; Fleck et al., 2019) to the data of Hauff et al. (2000) and Hoernle et al. (2004) data, a Fish Canyon sanidine age of 28.099 ± 0.013 Ma (FCs; (1σ; Fleck et al., 2019) to the Madrigal et al. (2015) data, and a Fish Canyon Tuff biotite age of 28.06 Ma (FCT-3; Kuiper, Deino, & Hilgen, 2008) was applied to the Sinton et al. (1997) data. The recalculated ^{40}Ar/^{39}Ar ages are quoted Figure 1 in Tables 1-2. ^{40}Ar/^{39}Ar dating of samples CR01 and CR03 yielded plateau ages of 131.0 ± 3.2 Ma (61.0% 39Ar; MSWD = 0.41, P = 93%) and 130.0 ± 4.5 Ma (67.8% ^{39}Ar; MSWD = 0.41, P = 96%), respectively. Both age spectra are disturbed, and high Cl concentrations (monitored by the analysis of the mass 35.5 baseline value) were observed in many steps. Initial step-heating analyses yielded very high quantities of atmospheric ^{40}Ar, and overall both samples show quite high atmospheric ^{40}Ar concentrations of 26-99% (CR01) and 35-99% (CR03), which suggests that the basaltic glass samples may have been affected by alteration. These factors may explain the large age uncertainties observed in some steps of both samples (Table DR2). Inverse isochrons plots from the plateau steps of each sample yielded isochron ages within 2σ uncertainties of the plateau ages: 130 ± 11 Ma (CR01; 95% confidence (95% conf.); MSWD = 0.48, P = 87, with an unacceptable Spreading Factor (SF) value of 25.1%), and 136 ± 11 Ma (CR03; 95% conf.; MSWD = 0.33; P = 98%, with an acceptable SF value of 41.0%). Both samples yielded initial ^{40}Ar/^{36}Ar ratios of 297 ± 12 (CR01) and 288 ± 13 (CR03), within 95% conf. uncertainties of the atmospheric ^{40}Ar/^{36}Ar ratio of 295.5 (Steiger & Jäger, 1977; Tables DR1 and DR2, Supplementary material).

4.2 Paleointensity results

Overall, 21 of the 360 specimens and 4 of the 42 sites analysed passed the strict selection criteria (CCRIT-strict, Table 2), while 69 of 360 specimens and nine of the 42 sites passed the modified CCRIT (Paterson et al., 2014) (CCRIT-relaxed, with a FRAC greater than 0.3; Table 2), with an overall 6 and 20% success rate at the specimen level.

The main reason for failure (77% of specimens) was a combination of criteria which together indicated alteration of the sample, as shown by failed pTRM checks, segmented or curved Arai plots (e.g. Figure 3b) suggesting the presence of multidomain-like grains and random and chaotic behavior (30.5%). 12% of the specimens failed the FRAC criterion because of the presence of multi-components of the remanent magnetization (e.g., Figure 3d). A further 11% failed because of k', thought to reflect a threshold separating single-domain-like from multidomain-like remanences. In case of evidence of multiple components of remanent magnetization observed on some of the Zijderveld diagrams (for instance, Figure 3c; Zijderveld, 1967), we selected only the temperature steps corresponding to the characteristic remanent magnetization (ChRM) component heading towards the origin of the Zijderveld. For these specimens, we relaxed the FRAC criterion to 0.3. For instance, Figure 3d shows a Zijderveld diagram that clearly indicates two components, a low temperature (NRM to 300°C) and the ChRM from 350 to 495°C heading towards the origin. Overall, the NRM values vary significantly from about 5.3 μAm^2 to 30 μAm^2 and the intensities vary from 21 μT to 37 μT (Table 2).

The swarm-violin plot (Figure 4a) shows the distribution of all specimens which passed the CCRIT-relaxed selection criteria at the specimen level (Table 2). Of the fourteen sites, only three (CR03, CR18, and NC01) have two or three specimens. Specimens from three sites (CR01, CR06 and CR14) show a high dispersion distribution. The remaining eight sites (CR02, CR05, CR06, NC02, NC03 and NC17) show a low dispersion of the density distribution, are symmetric around their mean values and are the only specimens passing the CCRIT-relaxed site level selection criteria. When the strictest CCRIT-strict criteria are applied (Table 2 and Figure 4b), three sites are characterised by only two specimens, (CR02, CR03 and NC03) while sites CR13 and CR20 shows a high dispersion distribution and a σ% greater than 25%, thus they do not pass the strict selection criteria. Finally, site CR14 is characterized by a σ% of 23%, thus it can be considered reliable.

Site	Age (Ma)	n/N	B (μT)	σ (%)	Lat (°N)	VADM	VADM1
strict							
CR06	112.4 ± 0.9	7/24	33.7 ± 3.9	11.6	3.6	86.6 ± 10.0	83.0 ± 9.6
CR05	112.4 ± 0.9	6/18	20.7 ± 3.2	15.6	3.6	53.2 ± 8.2	51.0 ± 7.8
NC17	121.4 ± 1.1	3/8	21.3 ± 1.2	5.6	9.5	53.0 ± 3.0	52.8 ± 3.0
CR14	135.1 ± 1.5	5/24	34.4 ± 8.1	23.0	3.6	88.4 ± 20.0	84.8 ± 19.9
relaxed							
CR06	112.4 ± 0.9	13/24	32.9 ± 3.8	11.6	3.6	84.6 ± 9.7	81.1 ± 9.4
CR05	112.4 ± 0.9	16/18	20.37 ± 5.0	23.8	3.6	52.2 ± 12.6	50.0 ± 12.3
NC02	113.0 ± 3.5	6/17	29.0 ± 7.0	24.2	1.5	74.9 ± 18.1	71.3 ± 17.2
NC03	113.0 ± 3.5	9/18	37.4 ± 7.4	19.6	1.5	96.6 ± 19.1	91.9± 18.1
NC17	121.4 ± 1.1	6/8	21.8 ± 5.9	26.9	9.5	54.2 ± 14.6	54.0 ± 14.6
CR18	121.4 ± 1.1	3/10	32.3 ± 3.2	9.8	9.5	80.4 ± 8.0	80.0 ± 7.9
CR03	130.0 ± 4.5	3/12	32.3 ± 0.6	1.9	3.6	83.0 ± 1.5	79.6 ± 1.5
CR14	135.1 ± 1.5	12/24	32.9 ± 7.3	22.3	3.6	84.6 ± 18.7	81.1 ± 17.9
CR02	141.0 ± 0.9	4/6	21.4 ± 2.0	3.6	3.6	55.0 ± 5.4	52.7 ± 5.1

Table 2. Paleointensity results from Costa Rica obtained with the CCRIT-strict selection criteria, and CCRIT-relaxed with a FRAC value greater than 0.3. The ^{40}Ar/^{39}Ar ages are shown with 2σ uncertainties). Abbreviations: n/N = number (n) of specimens yielding a reliable paleointensity signal and total number of specimens analysed (N), B = paleointensity values. Lat (°N)= paleolatitude reported by Boshman et al. (2019), VADM and VADM1 = Virtual Axial Dipole Moment values (ZAm^2=10^{21} Am^2) calculated using the Boshman et al. (2019) paleolatitudes and present day latitudes, respectively. Sites for which no paleointensity could be obtained are omitted from this table.

At the site level (Figure 5), intensities before the onset of the CNS ($\sim$ 141 Ma) are low and and similar to the values around the onset of the CNS ($\sim$121, sites NC17 and CR02). After the onset of the CNS the intensity values vary between 20 $\pm$ 4 μT (site CR05) and 37 $\pm$ 7 μT (site NC03), with an average of 29 $\pm$ 7 μT.

5 Discussion

In total, reliable paleointensity estimates have been obtained for four sites from Costa Rica, with ages spanning a 23 Ma interval between 135 and 112 Ma, using the CCRIT-strict selection criteria and nine sites spanning 145 to 112 Ma using the CCRIT-relaxed criteria (Table 2, Figure 5). Of the successful sites passing the CCRIT-strict criteria (Table 2), two are from the early CNS (112 Ma), one is close to the CNS onset (121 Ma) and one is from the pre-CNS (135 Ma). Of the successful sites passing the CCRIT-relaxed criteria (Table 2), three are from the pre-CNS (145-130 Ma), two are close to the CNS onset (121 Ma) and four are from the early CNS (113-112 Ma). In order to compare our results from Costa Rica to all the other data from similar ages, we calculated the virtual axial dipole moments (VADMs), using both paleolatitudes from the study of Boshman et al. (2019) (VADM; Table 2 and Figure 5) and the present-day latitude (VADM1; Table 2 and Figure 5), between 9 and 10° N (Table 1). The paleolatitudes reported by Boshman et al. (2019) range between 1 and 9° N (Table 2). These VADMs values are systematically slightly higher than the VADM1s values, but statistically indistinguishable (overlapping within the quoted 1σ errors). When we consider our results obtained with the CCRIT-strict criteria, one site with an age of 135 Ma gives reliable intensity results of 34 $\pm$ 8 μT (equivalent to a paleomagnetic dipole moment, PDM, of 88 $\pm$ 20 ZAm^2), while one site with an age of 121 Ma gives a value of 21 $\pm$ 1 μT (or 53 $\pm$ 3 ZAm^2 during the onset of the CNS and two sites with ages of 112 give variable intensity values ranging from 21 $\pm$ 3 to 34 $\pm$ 4 μT (or 53 $\pm$ 8 to 87 $\pm$ 10 ZAm^2) after the onset of the CNS. Considering the results obtained with the CCRIT-relaxed criteria, the average paleointensity value from Costa Rica during the CNS is $\sim$ 29 μT ($\sim$77 ZAm^2), whereas the pre-CNS records a lower intensity value of 21 $\pm$ 1 μT (or VADM of 53 $\pm$ 3 ZAm^2). Unfortunately, the recognition of any trend is limited by the lack of data between 135-121 and 121-112 Ma, around the onset of the CNS.

In order to verify the polarity and the reliability of the close-proximity geochronological ages assigned to our sites, (CNS sites are expected to have normal polarities), we tried to compare the directional data of Boshman et al. (2019), which were obtained from the same locations as this study. Unfortunately, our sampling did not include drilling oriented core samples. In addition, all of Boshman et al. (2019) sites (except for a few that failed a fold test) are interpreted as having normal polarity, including the sampling site near our CR14 site , which was ^{40}Ar/ ^{39}Ar dated at 135.1 $\pm$ 1.5 Ma (Hoernle et al., 2004). Therefore, the directional information by Boshman et al. (2019) cannot provide a test of the ^{40}Ar/ ^{39}Ar ages. Data from this study (shown as red and black stars, for results obtained using the CCRIT-strict and CCRIT-relaxed, respectively, in Figure 6) display similar to lower values than the present-day field (red dashed line in Figure 6, calculated using the International Geomagnetic Reference Field (IGRF) model, and equal to or slightly higher than the average value of 50 ZAm^2 previously obtained for the CNS (blue solid line in Figure 6, Bol'shakov & Solodonikov, 1983; Pick & Tauxe, 1993a; Zhu et al., 2001; Zhu, Hoffman, et al., 2004). In order to compare the new paleointensity data from Costa Rica with the existing database, we adopted a consistent approach. We re-analysed the available data using the same set of CCRIT-relaxed criteria, as employed in this study. Only five studies published the original measurement data, following the FAIR, or Findability, Accessibility, Interoperabilty and Reusability, principles (Wilkinson et al., 2016). After our re-analyses, fewer sites were found to pass the CCRIT-relaxed selection criteria compared to the results of the original studies. From the study of Zhu et al., 2008, 73% (25 of 34) of the original sites pass CCRIT-relaxed criteria. In the study of Tauxe and Staudigel (2004), only 23% (9 of 39) of the sites pass. In Figure 6, we plot all the available data for the last 200 Ma from the MagIC database as grey circles, and the reinterpreted data from literature as orange, green, pink, blue and purple circles (Tauxe & Staudigel, 2004; Granot et al., 2007; Zhu et al., 2008; Tauxe et al., 2013; Tauxe, 2006), respectively. The Costa Rica paleointensity values are similar to the 114-110 Ma Sohongtu values obtained by Zhu et al. (2008) and to the re-interpreted late-CNS mean values obtained for the late CNS after re-interpreting the data from the SBG Troodos ophiolite (92 Ma; Tauxe and Staudigel 2004; Granot et al., 2007). Indeed, we obtained average re-calculated values of 65.4 ZAm^2 (Tauxe & Staudigel, 2004) and 55.9 ZAm^2 (Granot et al., 2007)(orange and green circles in Figure 6).

The average Costa Rica paleointensity values is $\sim$ 13 ZAm^2 higher than the values of the long-term average of 42 ZAm^2 suggested by Juarez et al. (1998) but is similar to the mean value of $\sim$50 ZAm^2 calculated using the entire MagIC database from the last 200 Ma. These results appear to contradict the suggestion by Selkin and Tauxe (2000) that the distribution of paleointensities does not change substantially between 124 and 30 Ma (low reversal rate) and 30-0.3 Ma (high reversal rate). At the same time, our data do not seem to support the hypothesis that long periods of low reversal frequency are characterized by a stronger field than periods of high reversal rates (Tauxe & Hartl, 1997; Constable et al., 1998). Is is worth noticing that the re-analysis of SBG samples from DSDP and ODP drill cores compiled by Tauxe (2006) from 0 to 122 Ma suggests a consistently weaker field than previously reported and provide low values at both the onset and toward the end of the CNS. Together, Costa Rica and the Troodos ophiolite data show a relatively weak field just before the onset of the CNS (around 121 Ma) but a stronger field both during the first 20 Ma and towards the end of the CNS. The paucity of data between 110 and 95 Ma hampers the interpretation of any paleointensity field trend during the middle part of the CNS.

Monte Carlo simulations, using the TK03 paleosecular variation model of Tauxe and Kent (2004), show that at least 25 estimates for a given age are required to robustly estimate paleofield strength value (Tauxe & Staudigel, 2004). Unfortunately, none of the individual studies available so far have sufficient temporal sampling to provide a robust estimate of the paleofield strength during the CNS.

Indeed, a robust record of reversals and excursions is needed, along with a reliable and temporally and spatially well distributed paleointensity dataset in order to verify a possible correlation between dipole strength and reversal frequency. This in turn, would provide important constraints on the heat flux across the Earth's core-mantle boundary, the energy states of the geodynamo and their modelling (Biggin et al., 2012). The new, reliable and robust paleointensity data from Costa Rica contribute significantly to the current dataset and can be used in future numerical simulations in order to understand long-term variations, the geomagnetic field features and whether these are a result of external forcing mechanisms and/or reflect the hydrodynamic processes occurring in the Earth's mantle, outer core and inner core.

6 Conclusions

This study provides high-quality paleointensity data from 13 sites Costa Rica, spanning 23 Ma of volcanic activity, between 135 and 112 Ma, from before the onset of the CNS and during the beginning of the CNS.

- We investigated 42 submarine basaltic glass (SBG) sites from pillow lava margins, sampled along the coast from the upper crust sequences of the Murciélago Islands and Nicoya ophiolite, from the north, north-west, and the south of the Nicoya Peninsula.

- New ^{40}Ar/^{39}Ar ages are presented, and, along with ^{40}Ar/^{39}Ar and biostratigraphic ages from previous studies, indicate ages ranging from 141 to 94 Ma.
- We present new high-quality paleointensity results from four sites, with ages from 135 to 112 Ma, obtained using the IZZI protocol and applying a CCRIT-strict selection criteria.
- Allowing interpretation of two-component magnetization by relaxing the FRAC criterion (CCRIT-relaxed) resulted in the inclusion of an additional nine sites with ages from 141 Ma to 112 Ma.
- The new paleointensity data from before the onset of the CNS (135 Ma) yield a value of 34 ± 8 μT (or a PDM value of 88 ± 20 ZAm^2), one paleointensity value for the onset of the CNS at 121 Ma (21 ± 1 μT or 53 ± 3 10 ZAm^2), and two paleointensity values from the first part of the CNS vary from 21 ± 3 to 34 ± 4 μT (or 53 ± 8 to 87 ± 10 ZAm^2).
- These new CNS paleointensity results from Costa Rica are similar to the values from the 114-110 Ma Suhongtu lava section, Inner Mongolia, of ∼ 50 ZAm^2 (Zhu et al., 2008) and the ∼92 Ma Troodos Ophiolite, re-interpreted using the same strict criteria as in this study, of ∼55 ZAm^2 (Granot et al., 2007), but are lower than the Troodos Ophiolite paleointenisty value of ∼65 ZAm^2 by Tauxe and Staudigel (2004).
- The new Costa Rica data indicate that the strength of the geomagnetic field was relatively lower during the onset of the CNS and higher in the early CNS, but all these values are higher than the average geomagnetic field strength. Finally, our data do not seem to support a correlation between the strength and stability of the geomagnetic field.
- These new paleointensity results can contribute to understanding long-term variation and features of the Earth's Magnetic Field.

Acknowledgments

Data will be made available on the MagIC database: https://earthref.org/MagIC/16870/d197f16c-70ef-459a-98c1-f8f67f757731). This work was supported in part by NSF Grant EAR1547263 to LT, and NEXT Data grant to FF and ADC. KH received funds from the GEOMAR Research Center. We thank Jan Sticklus for his help with the ^{40}Ar/^{39}Ar dating of samples at GEOMAR Helmholtz Centre for Ocean Research Kiel.

References

Aitken, M. J., Allsop, A. L., Bussell, G. D., & Winter, M. B. (1988). Determination of the intensity of the Earth's magnetic field during archeological times: reliability of the Thellier technique. *Rev. Geophys.*, *26*, 3–12.

Azema, J., Tournon, J., & Sornay, J. (n.d.). Presencia de amonites del Albiano Superior en las formaciones del Complejo de Nicoya. El yacimiento de Loma Chumico, provincia de Guanacaste, Costa Rica, volume = 2, year = 1978. *Inf. Sem. IGN*, 71–76.

Bandini, A. N., Flores, K., Baumgartner, P., Jackett, S. J., & Denyer, P. (2008). Late Cretaceous and Paleogene radiolaria from the Nicoya Peninsula, Costa Rica: a tectonostratigraphic application. *Stratigraphy*, *5*, 3-21.

Baumgartner, P. (1984). El complejo ofiolíicoya (Costa Rica): Modelos estructurales analizados en funcíón de las edades de los Radiolarios (Calloviense a Santoniense). In: Spechmann, P., Ed. Manual de Geolígíioíítico de Nicoya (Costa Rica): Modelos estructurales analizados enófónóión de las edades de los Radiolarios (Calloviense a Santoniense). In: Spechmann, P., Ed. *Manual de Geología de Costa Rica, Universidad de Costa Rica*, 115-123.

Baumgartner, P., O'Dogherty, L., Goričan, Š., Urquhart, E., Pillevuit, A., &

De Wever, P. (1995). Middle Jurassic to Lower Cretaceous radiolaria of Tethys: occurrences, systematics, biochronology.
Baumgartner-Mora, C., & Denyer, P. (2002). Campanian-Maastrichtian limestone with larger foraminifera from Peñruja Rock (Santa Elena Peninsula). *Revista Geolóérica Central*, *26*, 85-89.
Biggin, A., & McCormack, A., A.and Roberts. (2010). Paleointensity database updated and upgraded. *Eos, Transactions American Geophysical Union*, *91*(2), 15–15.
Biggin, A., Steinberger, B., Aubert, J., Suttie, N., Holme, R., Torsvik, T. H., ... van Hinsbergen, D. (2012). Possible links between long-term geomagnetic variations and whole-mantle convection processes. *Nature Geoscience*, *5*, 526-533.
Biggin, A., & Thomas, D. N. (2003). Analysis of long-term variations in the geomagnetic poloidal field intensity and evaluation of their relationship with global geodynamics. *Geophys. J. Int.*, *152*(2), 392-415.
Bol'shakov, A., & Solodonikov, G. M. (1983). Geomagnetic field intensity in Armenia in the Late Jurassic and Early Cretaceous. *Izv. Earth Physics*, *19*, 976-982.
Boshman, L., van der Wiel, E., Flores, K., Langereis, C., & van Hinsbergen, D. (2019). The Caribbean and Farallon plates connected: Constraints from stratigraphy and paleomagnetism of the Nicoya Peninsula, Costa Rica. *J. Geophys. Res.-Solid Earth*, *123*, 6243-6266. doi: 10.1029/2018JB016369
Bowles, J., Gee, J. S., Burgess, K., & Cooper, R. F. (2011). Timing of magnetite formation in basaltic glass: Insights from synthetic analogs and relevance for geomagnetic paleointensity analyses. *Geochem. Geophys. Geosys.*, *12*(2).
Bowles, J., Gee, J. S., Kent, D., Bergmanis, E., & Sinton, J. (2005). Cooling rate effects on paleointensity estimates in submarine basaltic glass and implications for dating young flows. *Geochem. Geophys. Geosys.*, *6*, Q07002, doi:10.1029/2004GC000900.
Brown, M., Korte, M., Holme, R., Wardinski, I., & Gunnarson, S. (2018). Earth's magnetic field is probably not reversing. *Proc. Nat. Acad. Sci.*, *115*, 5111-5116. doi: 10.1073/pnas.1722110115
Carlut, J., & Kent, D. (2000). Paleointensity record in zero-age submarine basalt glass: Testing a new dating technique for recent MORBS. *Earth Planet. Sci. Lett.*, *183*, 389-401.
Cejudo Ruiz, R., Goguitchaichvili, A., Morales, J., Trindade, R., Alva Valdivia, L., & Urrutia-Fucugauchi, J. (2009). Absolute Thellier paleointensities from Ponta Grossa dikes (southern Brazil) and the early Cretaceous geomagnetic field strength. *Geof. Int.*, *48*, 243-252.
Channell, J., Singer, B., & Jicha, B. (2020). Timing of Quaternerary geomagnetic reversals and excursions in volcanic and sedimentary archives. *Quat. Sci. Rev.*, *228*. doi: 10.1016/j.quascirev.2019.106114
Coe, R. S. (1967). The determination of paleo-intensities of the Earth's magnetic field with emphasis on mechanisms which could cause non-ideal behavior in Thellier's method. *J. Geomag. Geoelectr.*, *19*, 157–178.
Coe, R. S., Grommé, S., & Mankinen, E. A. (1978). Geomagnetic paleointensities from radiocarbon-dated lava flows on Hawaii and the question of the Pacific nondipole low. *J. Geophys. Res.*, *83*, 1740–1756.
Constable, C. G., Tauxe, L., & Parker, R. L. (1998). Analysis of 11 Myr of geomagnetic intensity variation. *J. Geophys. Res.-Solid Earth*, *103*(B8), 17735-17748.
Cottrell, R. D., & Tarduno, J. (2000). In search of high-fidelity geomagnetic paleointensities: A comparison of single plagioclase cyrstal and whole rock Thellier-Thellier analyses. *J. Geophys. Res*, *105*, 23579-23594.
Courtillot, V., Gallet, Y., Le Mouël, J.-L., Futeau, F., & Genevey, A. (2007). Are there connections between the Earth's magnetic field and climate? *Earth Planet. Sci. Lett.*, *253*(328-339).

Cox, A. V. (1968). Lengths of geomagnetic polarity intervals. *J. Geophys. Res.*, *73*, 3247–3260.

Cromwell, G., Tauxe, L., & Halldórsson, S. (2015). New paleointensity results from rapidly cooled Icelandic lavas: Implications for Arctic geomagnetic field strength. *Journal of Geophysical Research: Solid Earth*, *120*(5), 2913–2934.

Cronin, M., Tauxe, L., Constable, C., Selkin, P., & Pick, T. (2001). Noise in the quiet zone. *Earth Planet. Sci. Lett.*, *190*, 13-30.

DeMets, C. (2001). A new estimate for present-day Cocos-Caribbean plate motion: Implications for slip along the Central American volcanic arc. *Geophys. Res. Lett.*, *28*, 4043-4046. doi: 10.1029/2001GL013518

Denyer, P., & Baumgartner, P. (2006). Emplacement of Jurassic-Lower Cretaceous radiolarites of the Nicoya Complex (Costa Rica). *Geologica Acta*, *4*, 203-218.

Denyer, P., & Gazel, E. (2009). The Costa Rican Jurassic to Miocene oceanic complexes: origin, tectonics and relations. *J. South Amer. Earth Sci.*, *28*, 429-442.

Dodd, S., Mac Niocaill, C., & Muxworthy, A. (2015). Long duration (>4 Ma) and steady-state volcanic activity in the early Cretaceous Paraná-Etendeka Large Igneous Province: New paleomagnetic data from Namibia. *Earth Planet. Sci. Lett.*, *414*, 16-29. doi: 10.1016/j.epsl.2015.01.009

Escuder-Viruete, J., Baumgartner, P. O., & Castillo-Carrión, M. (2015). Compositional diversity in peridotites as result of a multi-process history: The Pacific-derived Santa Elena ophiolite, northwest Costa Rica. *Lithos*, *231*, 16–34.

Fleck, R. J., Calvert, A. T., Coble, M. A., Wooden, J. L., Hodges, K., Hayden, L. A., … John, D. A. (2019). Characterization of the rhyolite of Bodie Hills and 40Ar/39Ar intercalibration with Ar mineral standards. *Chemical Geology*, *525*, 282–302.

Gallet, Y., & Hulot, G. (1997). Stationary and non-stationary behaviour within the geomagnetic polarity time scale. *Geophys. Res. Lett.*, *24*, 1875-1878.

Gee, J. S., & Kent, D. V. (2007). Source of oceanic magnetic anomalies and the geomagnetic polarity timescale. In M. Kono (Ed.), *Geomagnetism* (Vol. 5, p. 455-507). Elsevier.

Glazmaier, G. A., Coe, R. S., Hongre, L., & Roberts, P. H. (1999). How the Earth's mantle controls the frequency of geomagnetic reversals.

Goguitchaichvili, A., Cejudo Ruiz, R., Sanchez-Bettucci, L., Reyes, B., Valdivia, L. M. A., Urrutia-Fucugauchi, J., … Calvo-Rathert, M. (2008). New absolute paleointensity results from the Parana Magmatic Province (Uruguay) and the Early Cretaceous geomagnetic paleofield. *Geochem. Cosmochem. Acta.*, *9*. doi: 10.1029/2008GC002102

Granot, R., Dymont, J., & Gallet, Y. (2012). Geomagnetic field variability during the Cretaceous Normal Superchron. *Nature Geoscience*, *5*, 220-223.

Granot, R., Tauxe, L., Gee, J., & Ron, H. (2007). A view into the Cretaceous geomagnetic field from analysis of gabbros and submarine glasses. *Earth Planet. Sci. Lett.*, *256*, 1-11. doi: 10.1016/j.epsl.2006.12.028

Gubbins, D. (1999). The distinction between geomagnetic excursions and reversals. *Geophys. J. Int.*, *137*, F1-F3.

Hauff, F., Hoernle, K., van den Bogaard, P., Alvarado, G., & Garbe-Schönberg. (2000). Age and geochemistry of basaltic complexes in western Costa Rica: Contributions to the geotectonic evolution of Central America. *Geochem. Geophys. Geosys.*, *1*, doi:10.1029/1999GC000020.

Heller, R., Merrill, R. T., & McFadden, P. L. (2002). The variation of intensity of earth's magnetic field with time. *Phys. Earth Planet. Int.*, *131*(3-4), 237-249.

Helsley, C. E., & Steiner, M. B. (1968). Evidence for long intervals of normal polarity during the Cretaceous period. *Earth Planet. Sci. Lett.*, *5*, 325–332.

Hoernle, K., Hauff, F., & van den Bogaard, P. (2004). 70 m.y. history (139-69 Ma) for the Caribbean large igneous province. *Geology*, *32, doi: 10.1130/G20574.1*, 697-700.

Homrighausen, S., Hoernle, K., Hauff, F., Wartho, J.-A., van den Bogaard, P., & Garbe-Schönberg, D. (2019). New age and geochemical data from the Walvis Ridge: The temporal and spatial diversity of South Atlantic intraplate volcanism and its possible origin. *Geochimica et Cosmochimica Acta*, *245*, 16–34.

Hulot, G., Eymin, C., Langlais, B., Mandea, M., & Olsen, N. (2002). Small-scale structure of the geodynamo inferred from Oersted and Magsat satellite data. *Nature*, *416*, 620-623.

Hulot, G., & Gallet, Y. (2003). Do superchrons occur without any paleomagnetic warning? *Earth Planet. Sci. Lett.*, *210*, 191-201. doi: 10.1016/S0012-821X(03)00130-4

Ingham, E., Heslop, D., Roberts, A. P., Hawkins, R., & Sambridge, M. (2014). Is there a link between geomagnetic reversal frequency and paleointensity? A Bayesian approach. *J. Geophy. Res.*, *119*, 5290-5304. doi: 10.1002/2014JB010947

Juarez, M., & Tauxe, L. (2000). The intensity of the time averaged geomagnetic field: the last 5 m.y. *Earth Planet. Sci. Lett.*, *175*, 169-180.

Juarez, M., Tauxe, L., Gee, J. S., & Pick, T. (1998). The intensity of the Earth's magnetic field over the past 160 million years. *Nature*, *394*, 878-881.

Kent, D. V., & Gee, J. (1996). Magnetic alteration of zero-age oceanic basalt. *Geology*, *24*, 703-706.

Kuiper, K., Deino, A., & Hilgen, F. (2008). others, 2008. *Synchronizing rock clocks of Earth history: Science*, *320*, 500–504.

Kulakov, E., Sprain, C., Doubrovine, P., Smirnov, A., Paterson, G., Hawkins, L., ... Biggin, A. (2019). Analysis of an Updated Paleointensity Database (QPI-PINT) for 65–200 Ma: Implications for the Long-Term History of Dipole Moment Through the Mesozoic. *J. Geophys. Res.-Solid Earth*, *124*, 9999-10022. doi: 10.1029/2018JB017287

Larson, R. L., & Olson, P. (1991). Mantle plumes control magnetic reversal frequency. *Earth Planet. Sci. Lett.*, *107*, 437–447.

Loper, D. E., & McCartney, K. (1986). Mantle plumes and the periodicity of magnetic field reversals. *Geophys. Res. Lett.*, *13*, 1525–1528.

Madrigal, P., Gazel, E., Denyer, P., Smith, I., Jicha, B., Flores, K., ... Snow, J. (2015). A melt-focusing zone in the lithospheric mantle preserved in the Santa Elena Ophiolite, Costa Rica. *Lithos*, *230*, 189-205. doi: 10.1016/j.lithos.2015.04.015

Madrigal, P., Gazel, E., Flores, K., Bizimis, M., & Jicha, B. (2016). Record of massive upwellings from the Pacific large low shear velocity province. *Nature Communications*, *7*(13309). doi: 10.1038/ncomms13309

McElhinny, M., & Larson, R. (2003). Jurassic dipole low defined from land and sea data. *Eos Trans. AGU*, *84*, 362-366.

McFadden, P., & McElhinny, M. (1982). Variations in the geomagnetic dipole 2: statistical analysis of VDM's for the past 5 m.y. *Jour. Geomag. Geoelctr.*, *34*, 163-189.

McFadden, P., & McElhinny, M. (1984). A physical model for paleosecular variation. *Earth Planet. Sci. Lett.*, *67*(19-33). doi: 10.1111/j.1365-246X.1984.tb05072.x

McFadden, P., & Merrill, R. (2000). Evolution of the geomagnetic reversal rate since 160 Ma: Is the process continuous? *J Geophys Res-Solid Earth*, *105*, 28455-28460. doi: 10.1029/2000jb900258

Mercer, C. M., & Hodges, K. V. (2016). ArAr–A software tool to promote the robust comparison of K–Ar and 40Ar/39Ar dates published using different decay, isotopic, and monitor-age parameters. *Chemical Geology*, *440*, 148–163.

Moore, J. G., & Schilling, J.-G. (1973). Vesicles, water, and sulfur in Reykjanes Ridge basalts. *Contr. Mineral Petrol.*, *41*, 105-118. doi: 10.1007/bf00375036

Nagata, T., Arai, Y., & Momose, K. (1963). Secular variation of the geomagnetic total force during the last 5000 years. *J. Geophys. Res.*, *68*, 5277-5282.
Olierook, H., Jourdan, F., Whittaker, J., Merle, R., Jiang, Q., Pourteau, A., & Doucet, L. (2020). Timing and causes of the mid-Cretaceous global plate reorganization event. *Earth Planet. Sci. Lett.*, *534*, 1-13. doi: 10.1016/j.epsl.2020.116071
Olson, P., Christensen, U., & Driscoll, P. (2012). From superchrons to secular variation: A broadband dynamo frequency spectrum for the geomagnetic dipole. *Earth Planet. Sci. Lett.*, *319-320*, 75-82. doi: 10.1016/j.epsl.2011.12.008
Olson, P., & Hagay, A. (2015). Mantle superplumes induce geomagnetic superchrons. *Front. Earth Sci.*.
Paterson, G. (2011). A simple test for the presence of multidomain behavior during paleointensity experiments. *J. Geophys. Res.*, *116*(B10). doi: 10.1029/2011JB008369
Paterson, G., Tauxe, L., Biggin, A., Shaar, R., & Jonestrask, L. (2014). On improving the selection of Thellier-type paleointensity data. *Geochem. Geophys. Geosys.*, *15*(4). doi: 10.1002/2013GC005135
Pavón-Carrasco, F., & De Santis, A. (2016). The South Atlantic Anomaly: The Key for a Possible Geomagnetic Reversal. *Front. Earth Sci.,*, *4*, 40. doi: 10.3389/feart.2016.00040
Perrin, M., & Schnepp, E. (2004). IAGA paleointensity database: distribution and quality of the data set. *Phys. Earth Planet. Int.*, *147*(2-3), 255-267.
Perrin, M., & Shcherbakov, V. (1997). Paleointensity of the Earth's magnetic field for the past 400 Ma: evidence for a dipole structure during the Mesozoic low. *J. Geomag. Geoelectr.*, *49*, 601-614. doi: 10.5636/jgg.49.601
Pick, T., & Tauxe, L. (1993a). Geomagnetic paleointensities during the Cretaceous normal superchron measured using submarine basaltic glass. *Nature*, *366*, 238-242.
Pick, T., & Tauxe, L. (1993b). Holocene paleointensities: Thellier experiments on submarine basaltic glass from the East Pacific Rise. *Jour. Geophys. Res.*, *98*, 17949–17964.
Prévot, M., Derder, M. E. M., McWilliams, M., & Thompson, J. (1990). Intensity of the Earth's magnetic field: evidence for a Mesozoic dipole low. *Earth Planet. Sci. Lett.*, *97*, 129-139.
Riisager, P., Riisager, J., Zhao, X., & Coe, R. (2003). Cretaceous geomagnetic paleointensities: Thellier experiments on pillow lavas and submarine basaltic glass from the Ontong Java Plateau. *Geochem. Geophys. Geosyst.*, *4*(12), 8803, doi:10.1029/2003GC000611.
Santos, C., & Tauxe, L. (2019). Investigating the accuracy, precision, and cooling rate dependence of laboratory acquired thermal remanences during paleointensity experiments. *Geochem. Geophys. Geosys.*, *20*, 383-397. doi: 10.1029/2018GC007946
Schmidt-Effing, R. (1975). El primer hallazgo de amonites en Améácicas en dicha reóión. *Informe Semestral del Instituto Geográfico Nacional*, 53–61.
Schmidt-Effing, R. (1979). Alter und Genese des Nicoya Komplexes, einer ozeanischen Paläokruste (Oberjura bis Eozän) im südlichen Zentral Amerika. *Geol. Rundschau*, *68*, 457-494. doi: 10.1007/BF01820803
Selkin, P., & Tauxe, L. (2000). Long-term variations in paleointensity. *Phil. Trans. Roy. Soc. Lond.*, *358*, 1065-1088.
Sinton, C., Duncan, R. A., & Denyer, P. (1997). Nicoya Peninsula, Costa Rica: A single suite of Caribbean oceanic plateau magmas. *J. Geophy. Res.*, *102*, 15,507-15,520.
Smirnov, A. V., & Tarduno, J. A. (2003). Magnetic hysteresis monitoring of Cretaceous submarine basaltic glass during Thellier paleointensity experiments: evidence for alteration and attendant low field bias. *Earth Planet. Sci. Lett.*,

206(3-4), 571-585.

Steiger, R., & Jäger, E. (1977). Age and composition of the Rushan intrusive complex in the northern Sulu orogen, eastern China: petrogenesis and lithospheric mantle evolution. *Earth Planet. Sci. Lett.*, *36*, 359–62.

Tanaka, H., Kono, M., & Uchimura, H. (1995). Some global features of paleointensity in geological time. *Geophys. J. Int.*, *120*, 97–102.

Tarduno, J. A. (1990). Absolute inclination values from deep sea sediments: a reexamination of the Cretaceous Pacific record. *Geophys. Res. Lett.*, *17*, 101–104.

Tarduno, J. A., Blackman, E., & Mamajek, E. (2014). Detecting the oldest geodynamo and attendant shielding from the solar wind: Implications for habitability. *Phys, Earth. Planet. Int.*, *233*, 68-87.

Tarduno, J. A., & Cottrell, R. D. (2005). Dipole strength and variation of the time-averaged reversing and nonreversing geodynamo based on Thellier analyses of single plagioclase crystals. *J. Geophys. Res.*, *110*, doi:10.1029JB003970.

Tarduno, J. A., Cottrell, R. D., & Smirnov, A. V. (2001). High geomagnetic intensity during the mid-Cretaceous from Thellier analyses of single plagioclase crystals. *Science*, *291*(5509), 1779-1783.

Tarduno, J. A., Cottrell, R. D., & Smirnov, A. V. (2002). The Cretaceous superchron geodynamo: Observations near the tangent cylinder. *Proc. Natl. Acad. Sci. U. S. A.*, *99*(22), 14020-14025.

Tauxe, L. (2006). Long-term trends in paleointensity: The contribution of DSDP/ODP submarine basaltic glass collections. *Phys. Earth Planet. Int.*, *156*(3-4), 223-241.

Tauxe, L., Gee, J., Steiner, M., & Staudigel, H. (2013). Paleointensity results from the Jurassic: New constraints from submarine basaltic glasses of ODP Site 801C. *Geochem. Geophys. Geosys.*, *14*(10). doi: 10.1002/ggge/20282

Tauxe, L., & Hartl, P. (1997). 11 million years of Oligocene geomagnetic field behaviour. *Geophys. Jour. Int.*, *128*, 217-229.

Tauxe, L., & Kent, D. V. (2004). A simplified statistical model for the geomagnetic field and the detection of shallow bias in paleomagnetic inclinations: was the ancient magnetic field dipolar?

Tauxe, L., Shaar, R., Jonestrask, L., Swanson-Hysell, N., Minnett, R., Koppers, A. A. P., … Fairchild, L. (2016). PmagPy: Software package for paleomagnetic data analysis and a bridge to the Magnetics Information Consortium (MagIC) database. *Geochem. Geophys. Geosys.*, *17*. doi: 10.1002/2016GC006307

Tauxe, L., & Staudigel, H. (2004). Strength of the geomagnetic field in the Cretaceous Normal Superchron: New data from submarine basaltic glass of the Troodos Ophiolite. *Geochem. Geophys. Geosyst.*, *5*(2), Q02H06, doi:10.1029/2003GC000635.

Tauxe, L., & Yamazaki, T. (2015). Paleointensities. In M. Kono (Ed.), *Geomagnetism* (2nd Edition ed., Vol. 5, p. 461-509). Elsevier.

Thellier, E., & Thellier, O. (1959). Sur l'intensité du champ magnétique terrestre dans le passé historique et géologique. *Ann. Geophys.*, *15*, 285–378.

Thomas, D., Biggin, A., & Schmidt, P. (2000). A paleomagnetic study of Jurassic intrusives from southern New Sourth Wales: further evidence for a pre-Cenozoic dipole low. *Geophys. J. Int.*, *140*, 621-635.

Thomas, D., Rolph, T., Shaw, J., Gonzalez de Sherwood, S., & Zhuang, Z. (1998). Paleointensity studies of a late Permian lava succession from Guizhou Province, South China: implications for post-Kiaman dipole field behaviour. *Geophys. J. Int.*, *134*, 856-866.

Tournon, J., & Alvarado, G. (1997). *Mapa geológico de Costa Rica.* Ed. Tecnológica, Cartago.

Wang, H., Kent, D., & Rochette, P. (2015). Weaker axially dipolar time-averaged paleomagnetic field based on multidomain-corrected paleointensities from Galapagos lavas. *Proc. Nat. Acad. Sci.*, *112*, 15036-15041. doi: 10.1073/pnas.1505450112

Whattam, S. A., & Stern, R. J. (2016). Arc magmatic evolution and the construction of continental crust at the Central American Volcanic Arc system. *Int. Geol. Rev.*, *58*(6), 653–686.

Wilkinson, M. D., Dumontier, M., Aalbersberg, I. J., Appleton, G., Axton, M., Baak, A., ... others (2016). The FAIR guiding principles for scientific data management and stewardship. *Scientific data*, *3*.

Yu, Y., Tauxe, L., & Genevey, A. (2004). Toward an optimal geomagnetic field intensity determination technique. *Geochem. Geophys. Geosyst.*, *5*(2), Q02H07, doi:10.1029/2003GC000630.

Zhu, R., Hoffman, K. A., Nomade, S., Renne, P. R., Shi, R., Pan, Y., & Shi, G. H. (2004). Geomagnetic paleointensity and direct age determination of the ISEA (M0r?) chron. *Earth Planet. Sci. Lett.*, *217*(3-4), 285-295.

Zhu, R., Hoffman, K. A., Pan, Y., Shi, R., & Li, D. (2003). Evidence for weak geomagnetic field intensity prior to the Cretaceous normal superchron. *Phys. Earth Planet. Int.*, *136*, 187-199.

Zhu, R., Lo, C., Shi, R. P., Pan, Y. X., Shi, G. H., & Shao, J. (2004). Is there a precursor to the Cretaceous normal superchron? New paleointensity and age determination from Liaoning province, northeastern China. *Phys. Earth Planet. Int.*, *147*(2-3), 117-126.

Zhu, R., Pan, Y., He, H., Qin, H., & Ren, S. (2008). Paleomagnetism and ^{40}Ar/^{39}Ar age from a Cretaceous volcanic sequence, Inner Mongolia, China: Implications for the field variation during the Cretaceous normal superchron. *Phys. Earth. Planet. Int.*, *169*, 59-75. doi: 10.1016/j.pepi.2008.07.025

Zhu, R., Pan, Y. X., Shaw, J., Li, D. M., & Li, Q. (2001). Geomagnetic palaeointensity just prior to the Cretaceous normal superchron. *Phys. Earth Planet. Inter.*, *128*(1-4), 207-222.

Zijderveld, J. D. A. (1967). *A.C. demagnetization of rocks: Analysis of results.* Chapman and Hall.

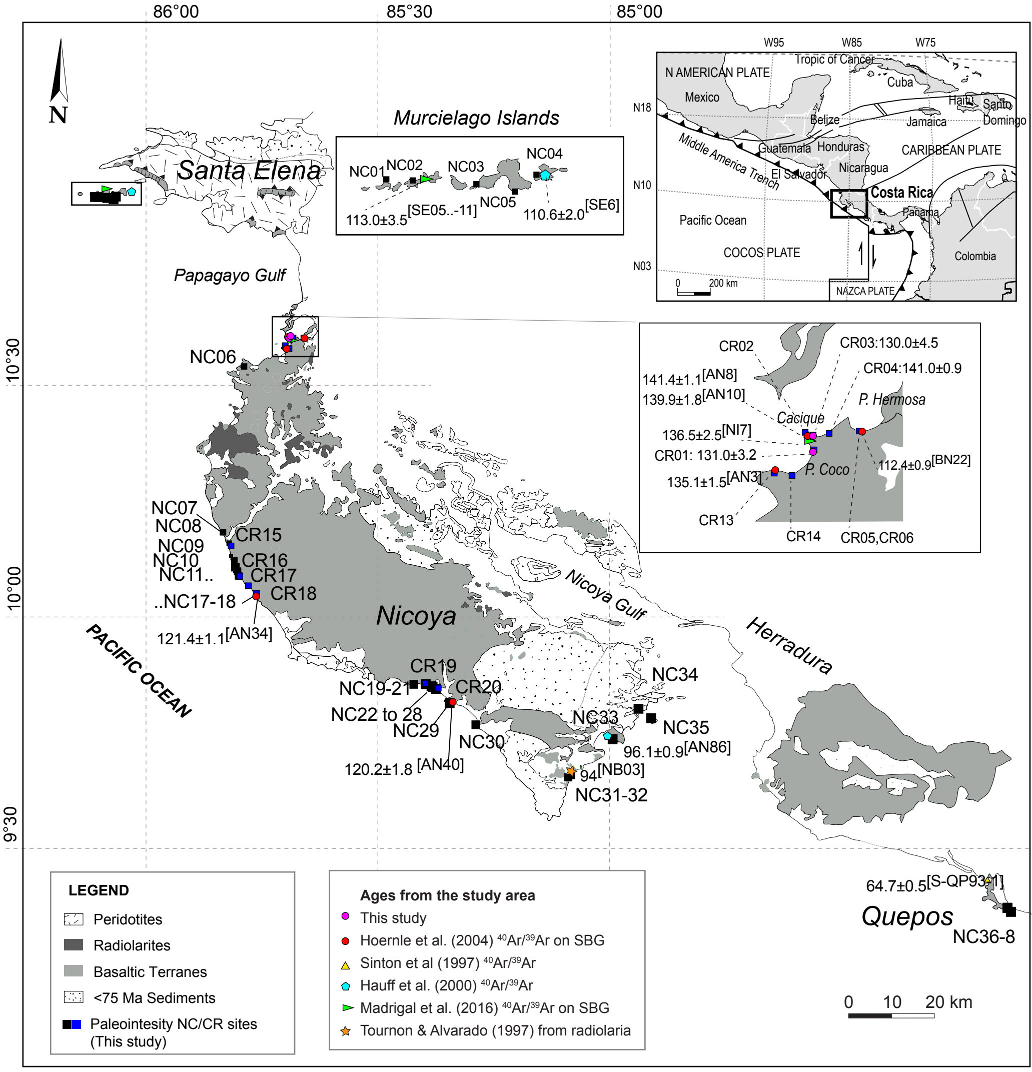

Figure 1. Geological map of the Nicoya Peninsula and surroundings, highlighting upper and lower crust terrains of the ophiolite, the sampling sites from previous studies and their age and the sites sampled for this study (black squares). Figure modified from Hauff et al. (2000). Sources of the ^{40}Ar/^{39}Ar ages are Sinton et al. (1997)and Hoernle et al. (2004), compiled by Denyer and Baumgartner (2006) and Denyer and Gazel (2009). The CR-labelled paleointensity sites are from SBG samples provided by K. Hoernle, while the NC- sites are from SBG collected in 2017 for this study.

Figure 2. Sampling of the Basaltic Glass (SBG) in pillow lavas from the Nicoya Peninsula and Murcielágo Islands (Costa Rica).

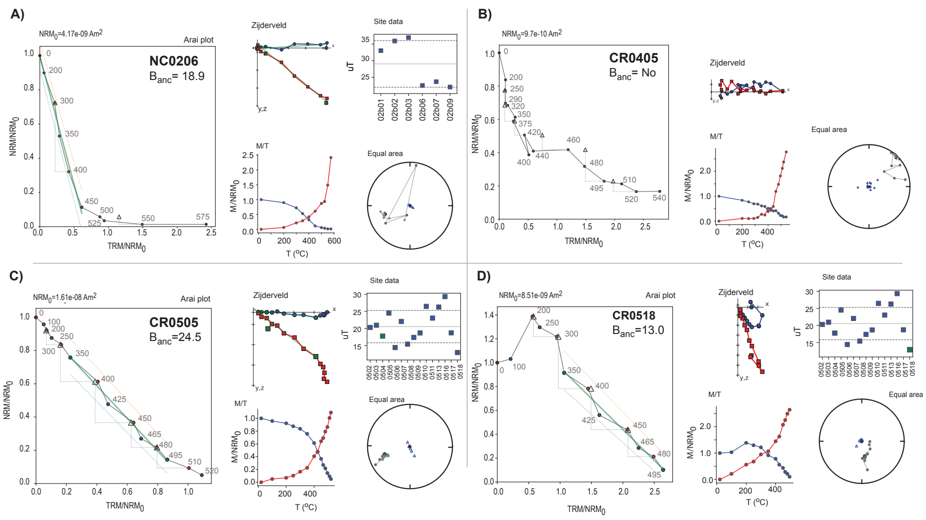

Figure 3. Examples of Arai plots (left hand plots in A-D) from four representative specimens, with relative Zijderveld (upper middle plots in A-D) magnetization vs. temperature (M/T; lower middle plots in A-D), equal area (lower right hand plots in A-D) and site-level plots (upper right hand plots in A-D). Numbers on the Arai plots are the Temperature steps (in $^\circ$ C), triangles show the directions of the pTRMs acquired in the laboratory field (along -z-axis of the specimens, i.e., the center of the diagram) and each blue and red circle a pair of ZI and IZ steps. Zijderveld diagrams are from un-oriented specimens and are plotted on the x-axis as the NRM direction with blue circles on the x,y plane and red squares in the x, z plane. The y-axis is with y,z as positive down. In the equal area plots, closed and open circles are the NRM directions in specimen coordinates with closed being the lower and upper hemisphere, respectively.

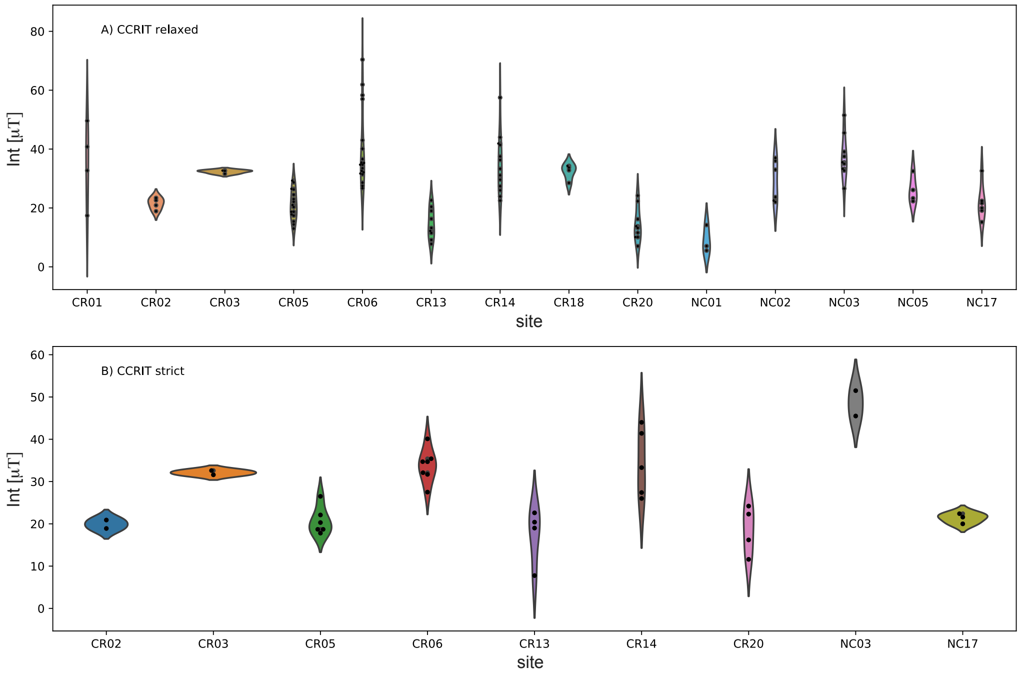

Figure 4. Violin plot showing intensity values for specimens (black dots) that passed the selection criteria along with kernel densities of their statistical distribution (colored areas), by using the A) CCRIT relaxed selection criteria, using a FRAC value greater than 0.3, and B) CCRIT strict criteria with a FRAC greater than 0.78.

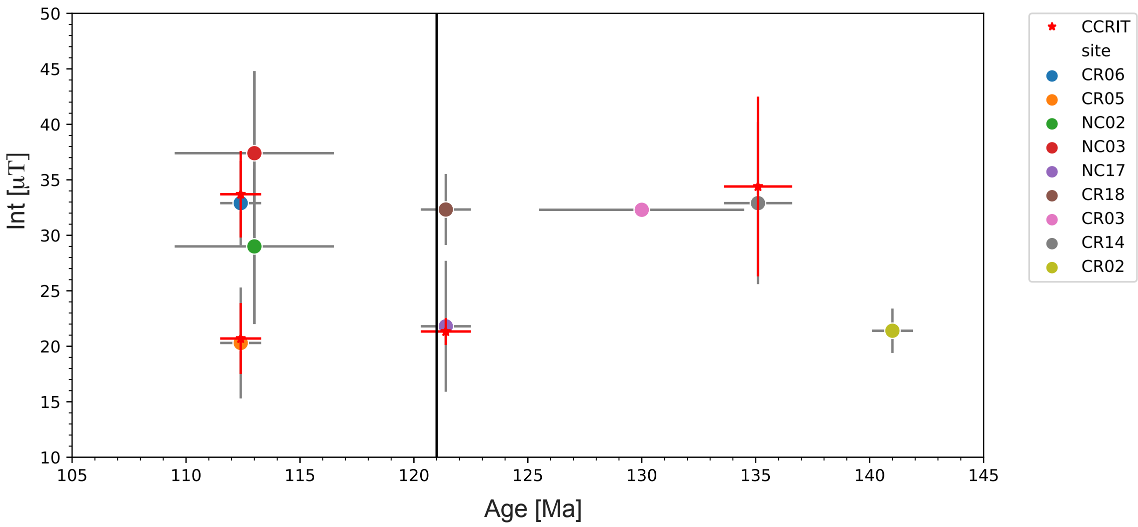

Figure 5. Paleointensity data (in μT) and the error bars (1σ μT) from Costa Rica sites vs Ages (Ma), obtained from ^{40}Ar/^{39}Ar dating. Red stars are the sites for which the paleointensity values were obtained using the CCRIT strict set of criteria. The CNS onset interval is marked with vertical black line.

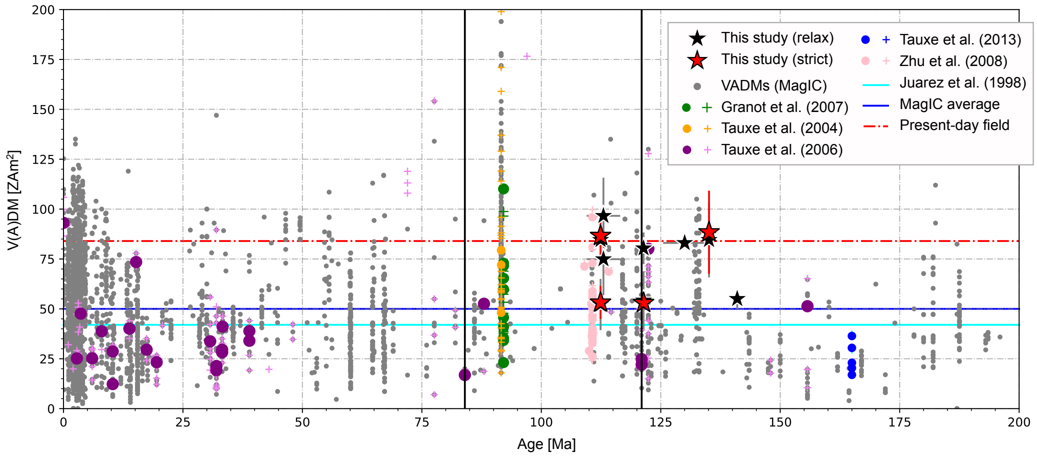

Figure 6. Black and red stars are the results of this study from Costa Rica (obtained with CCRIT relaxed and strict selection criteria, respectively). Grey dots represent the virtual (axial) dipole moments (V[A]DM) available in the MagIC database spanning the last 200 Ma. The bounds of the Cretaceous Normal Superchron (CNS) are indicated with vertical black lines. The strength of the present dipole field is shown as a dashed red line, the solid blue line represents the average of all MagIC data, and the long-term average of Juarez and Tauxe (2000); Tauxe et al. (2013) is shown as a solid aquamarine line. Circles are the data from submarine basaltic glass (SBG) re-analysed using the same criteria as this study, while the data as presented by the authors are marked as crosses.

DR Table 2 - $^{40}Ar/^{39}Ar$ data tables for samples CR01 and CR03 from Costa Rica

Sample #: CR01 glass

Step #	**Laser power (W)**	**$^{40}Ar/^{39}Ar$**	**$^{37}Ar/^{39}Ar$**	**$^{36}Ar/^{39}Ar$**	**$^{39}Ar_K$ (moles)**	**$^{40}Ar^*/^{39}Ar_K$**	**± 1σ**	**Ca/K**	**% $^{40}Ar_{atm}$**	**Fraction $^{39}Ar_K$**	**Age (Ma)**	**± 2σ (Ma)**
1	0.1	1250.0	1.55	4.190	6.34E-17	12.10	7.07	3.05	99.03	0.01	74.54	85.18
2	0.2	1170.0	10.60	3.890	1.45E-16	25.10	5.15	21.08	97.88	0.02	151.33	59.70
3	0.3	375.0	20.50	1.210	3.94E-16	19.70	2.10	40.97	94.85	0.07	119.82	24.73
4	0.4	134.0	22.90	0.403	7.90E-16	18.40	1.21	45.86	86.54	0.16	112.16	14.27
5	0.5	105.0	24.10	0.306	8.43E-16	17.80	0.92	48.35	83.41	0.26	108.61	10.93
6	0.6	105.0	28.50	0.295	7.75E-16	21.80	0.96	57.49	79.73	0.35	132.14	11.22
7	0.7	57.0	28.80	0.135	1.19E-15	21.50	0.77	58.11	63.24	0.49	130.39	9.00
8	0.8	63.3	28.90	0.156	8.52E-16	21.70	0.49	58.31	66.65	0.59	131.56	5.73
9	0.9	57.5	29.30	0.138	6.94E-16	21.10	0.81	59.16	64.36	0.67	128.04	9.54
10	1.0	57.2	29.90	0.137	5.57E-16	21.20	0.60	60.32	63.96	0.73	128.63	7.04
11	1.1	56.1	29.80	0.129	3.98E-16	22.40	0.95	60.02	61.20	0.78	135.64	11.09
12	1.2	54.3	29.90	0.121	3.34E-16	23.10	1.46	60.37	58.65	0.82	139.72	17.02
13	1.4	55.3	30.30	0.127	2.04E-16	22.40	2.80	61.1	60.70	0.84	135.64	32.72
14	1.5	56.8	31.00	0.130	1.20E-16	23.00	3.14	62.69	60.66	0.86	139.14	36.54
15	2.0	46.7	20.90	0.104	1.43E-16	19.00	3.01	41.69	60.16	0.87	115.70	35.57
16	3.0	25.0	11.20	0.046	5.00E-16	13.10	2.20	22.25	48.29	0.93	80.56	26.52
17	5.0	41.0	15.00	0.101	3.12E-16	13.40	2.17	29.78	67.73	0.97	82.36	26.05
18	10.0	20.7	5.72	0.058	1.41E-16	4.20	3.49	11.28	79.80	0.99	26.22	43.34
19	15.0	27.8	3.39	0.026	4.64E-17	20.50	10.10	6.66	26.41	0.99	124.53	118.18
20	20.0	24.7	0.64	0.052	7.78E-17	9.38	6.50	1.26	61.99	1.00	58.05	79.21

value	± % 2σ	Mass (mg)
####	0.257	1.565

Plateau steps are shown in bold.
Wt. % K = 0.52

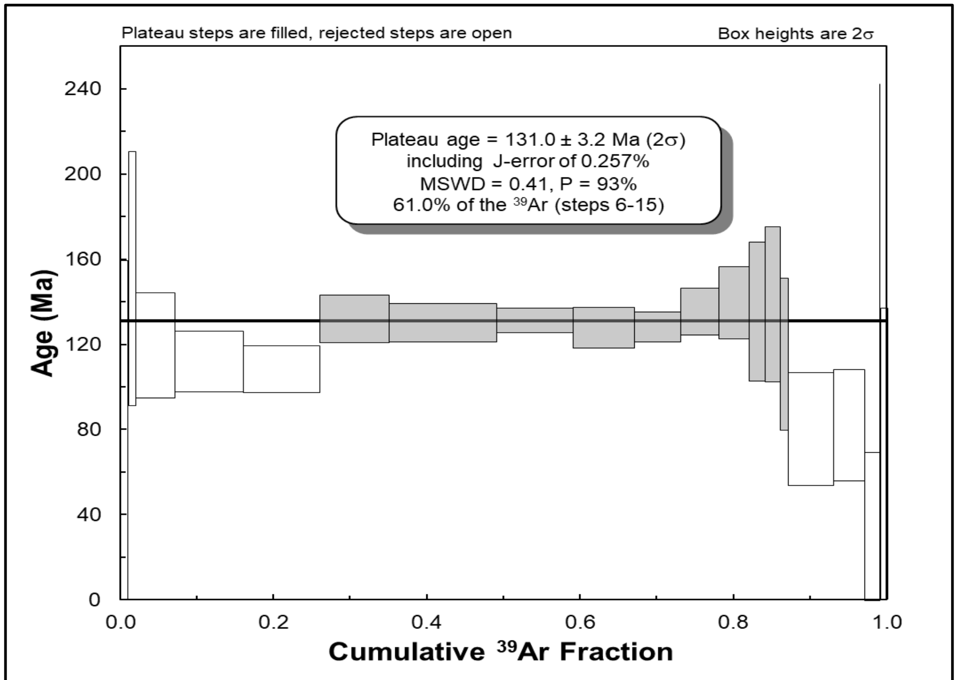

Plateau steps are filled, rejected steps are open
Box heights are 2σ
Plateau age = 131.0 ± 3.2 Ma (2σ)
including J-error of 0.257%
MSWD = 0.41, P = 93%
61.0% of the 39Ar (steps 6-15)
Age (Ma)
Cumulative 39Ar Fraction

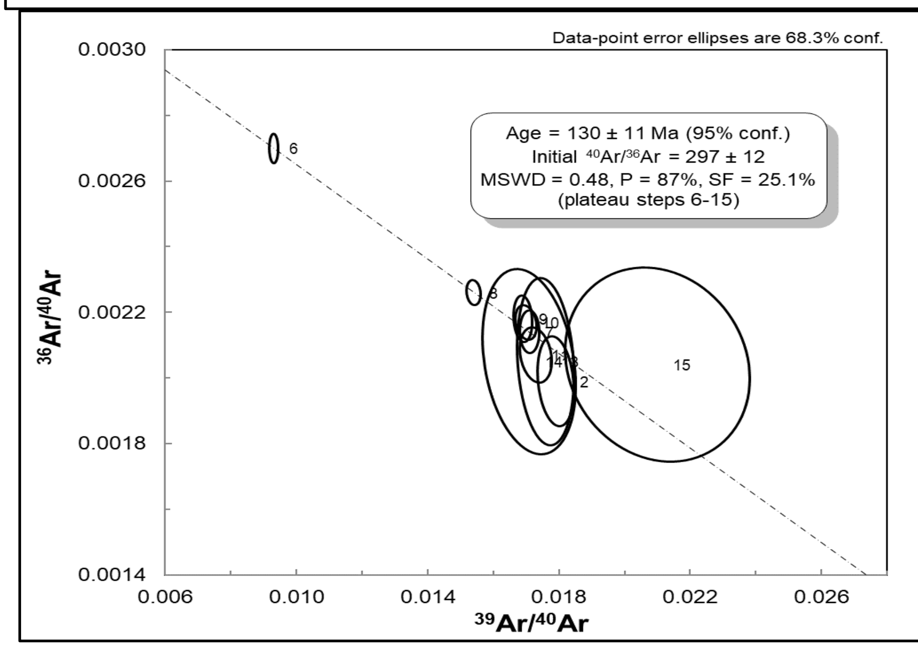

Data-point error ellipses are 68.3% conf.
Age = 130 ± 11 Ma (95% conf.)
Initial 40Ar/36Ar = 297 ± 12
MSWD = 0.48, P = 87%, SF = 25.1%
(plateau steps 6-15)
36Ar/40Ar
39Ar/40Ar

Sample #: CR03 glass

Step #	Laser power (W)	$^{40}Ar/^{39}Ar$	$^{37}Ar/^{39}Ar$	$^{36}Ar/^{39}Ar$	$^{39}Ar_K$ (moles)	$^{40}Ar^*/^{39}Ar_K$	± 1σ	Ca/K	% $^{40}Ar_{atm}$	Fraction $^{39}Ar_K$	Age (Ma)	± 2σ (Ma)
1	0.1	489.4	1.38	1.616	4.09E-16	12.10	4.29	2.70	97.53	0.04	74.52	51.85
2	0.2	781.0	3.36	2.606	4.03E-16	11.31	5.42	6.60	98.56	0.08	69.73	65.63
3	0.3	471.2	12.33	1.541	6.08E-16	17.58	2.10	24.45	96.31	0.14	107.29	24.88
4	0.4	137.9	22.50	0.413	8.48E-16	19.19	1.06	45.05	86.38	0.22	116.83	12.47
5	0.5	111.4	24.38	0.326	1.03E-15	18.61	1.02	48.91	83.68	0.32	113.42	12.05
6	0.6	98.2	27.39	0.277	1.11E-15	20.45	1.13	55.12	79.71	0.43	124.24	13.33
7	0.7	72.3	28.59	0.186	9.48E-16	21.56	0.98	57.59	70.97	0.52	130.76	11.50
8	0.8	62.2	28.72	0.153	9.47E-16	21.18	1.06	57.87	66.85	0.61	128.53	12.41
9	0.9	53.5	28.96	0.122	9.14E-16	21.76	0.83	58.36	60.45	0.70	131.90	9.67
10	1.0	47.7	29.60	0.105	8.09E-16	21.20	0.95	59.69	56.75	0.78	128.63	11.11
11	1.1	54.5	29.37	0.125	4.63E-16	21.88	1.30	59.22	60.96	0.83	132.60	15.22
12	1.2	56.9	32.48	0.134	2.69E-16	22.15	2.36	65.67	62.29	0.85	134.16	27.61
13	1.4	44.3	31.08	0.087	3.25E-16	23.30	2.22	62.76	48.96	0.89	140.86	25.85
14	1.5	61.2	30.96	0.156	2.13E-16	19.66	2.98	62.52	68.84	0.91	119.58	35.10
15	2.0	46.6	23.45	0.109	2.59E-16	17.98	2.83	46.99	62.29	0.93	109.69	33.54
16	3.0	34.8	21.72	0.051	2.99E-16	23.00	2.71	43.47	35.33	0.96	139.13	31.59
17	5.0	37.8	24.68	0.066	2.95E-16	22.11	2.14	49.54	42.88	0.99	133.98	25.01
18	10.0	43.2	22.59	0.070	1.07E-16	25.99	5.62	45.25	41.13	1.00	156.47	64.86

value	± % 2σ	Mass (mg)
####	0.257	1.903

Plateau steps are shown in bold.

Wt. % K = 0.51

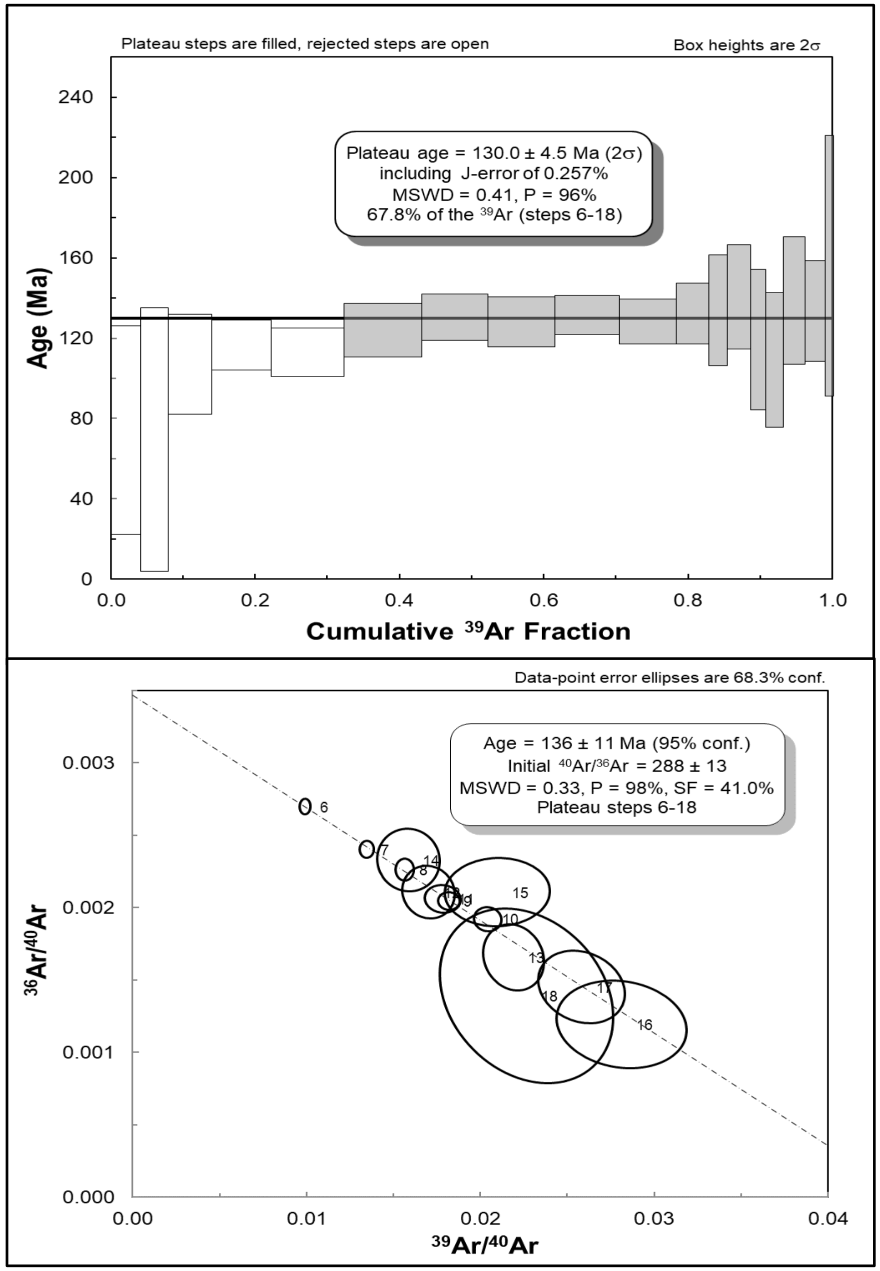

Plateau steps are filled, rejected steps are open
Box heights are 2σ
Plateau age = 130.0 ± 4.5 Ma (2σ)
including J-error of 0.257%
MSWD = 0.41, P = 96%
67.8% of the 39Ar (steps 6-18)
Age (Ma)
Cumulative 39Ar Fraction
Data-point error ellipses are 68.3% conf.
Age = 136 ± 11 Ma (95% conf.)
Initial 40Ar/36Ar = 288 ± 13
MSWD = 0.33, P = 98%, SF = 41.0%
Plateau steps 6-18
36Ar/40Ar
39Ar/40Ar